Published for SISSA by Springer

Received: June 9, 2025
Revised: October 3, 2025
Accepted: October 27, 2025
Published: December 10, 2025

Correlating lepton flavour violating $b \to s$ and leptonic decay modes in a minimal abelian extension of the Standard Model

P. Colangelo [a] **F. De Fazio** [a] **and D. Milillo** [a,b]

[a] *Istituto Nazionale di Fisica Nucleare, Sezione di Bari, Via Orabona 4, 70126 Bari, Italy*

[b] *Dipartimento Interateneo di Fisica "Michelangelo Merlin", Università degli Studi di Bari, via Orabona 4, 70126 Bari, Italy*

E-mail: pietro.colangelo@ba.infn.it, fulvia.defazio@ba.infn.it, davide.milillo@ba.infn.it

Abstract: We consider an abelian extension of the Standard Model (SM) comprising a new gauge group $\mathrm{U}(1)'$, with the neutral gauge boson Z' having flavour violating couplings to quarks and leptons. The fermion content is the same as in SM except for the addition of three right-handed neutrinos. The model, proposed in [1], describes the couplings of Z' to fermions in terms of three rational parameters $\epsilon_{1,2,3}$ that sum to zero imposing the cancellation of the gauge anomalies. Each ϵ_i is common to all fermions in a generation, a feature producing correlations among quark and lepton observables. We focus on $b \to s \ell_1^- \ell_2^+$ transitions for the lepton flavour conserving $\ell_1 = \ell_2$ and lepton flavour violating case $\ell_1 \neq \ell_2$. Small deviations with respect to the SM predictions are found in the first case, which reflects a feature of the model where quark and lepton sectors prevent each other to manifest large discrepancies with respect to SM. We investigate the correlations between rare B and B_s decays and the leptonic processes $\tau^- \to \mu^-\mu^+\mu^-$, $\mu^- \to e^-\gamma$, $\mu^- \to e^-e^+e^-$ and the $\mu^- \to e^-$ conversion in nuclei. We show that the current experimental upper bounds on these four channels play an increasingly important role in constraining the branching fractions of lepton flavour violating B and B_s decays. While the present bound on $\tau^- \to \mu^-\mu^+\mu^-$ does not impose significant restrictions, the other three modes set progressively more stringent limits, an important information for the planned new experimental facilities.

Keywords: Bottom Quarks, Lepton Flavour Violation (charged), New Gauge Interactions, Rare Decays

ArXiv ePrint: 2506.02552

https://doi.org/10.1007/JHEP12(2025)069

Contents

1 Introduction

The Standard Model of particle physics (SM) has been directly probed up to the energies accessible by the Large Hadron Collider and, within the present theoretical and experimental accuracy, the tests have been successful: the model provides us with a careful description of the interactions among the basic constituents of matter, excluding gravity. However, there are well known and broadly shared arguments to assert that this is not the ultimate theory for the fundamental interactions. Apart from the missing description of gravity, this model does not give any insight, for example, on the large number of independent parameters and the hierarchical structure of some of them, the regularities in the fermion sector, e.g. the organisation in generations, the texture of the fermion mixing matrices, and so on. A theory extended at higher energies, able to face at least some of the unsolved issues is actively sought for. The Standard Model would be its low-energy realisation.

The perspective for physics beyond the Standard Model (BSM) is reinforced by tensions emerged between some SM predictions and measurements. At present they do not reach the needed significance to claim the failure of the theory, but all together they could hint new physics (NP). Some tensions show up in the flavour sector (the *flavour anomalies*), identifying flavour physics as a path to disclose the BSM dynamics. Indeed, in flavour processes energy scales much higher that those directly accessed at colliders can be probed, in modes where heavy particles contribute as virtual states. To fully exploit this possibility, progress is required in the theoretical precision, as well as the increase in luminosity of the experimental facilities.

The flavour changing neutral current (FCNC) modes are of particular interest. In the SM they are forbidden at tree-level, as a consequence of the universality of the weak interactions and of the unitarity of the Cabibbo-Kobayashi-Maskawa matrix (CKM) rotating quark flavour eigenstates to mass eigenstates.[1] Among the tensions, there are indeed anomalies in observables related to the FCNC $b \to s$ transition. Moreover, there are difficulties concerning the value of some CKM matrix elements. Hints of violation of lepton flavour universality have also been spotted. A more detailed list of discrepancies includes [3, 4]:

- Tensions related to the CKM matrix elements $|V_{cb}|$ and $|V_{ub}|$. In both cases the value measured from exclusive decay modes (namely $B \to D^* \mu \bar{\nu}_\mu$ and $B \to \pi \mu \bar{\nu}_\mu$) is smaller than the value obtained from the inclusive $B \to X_{c,u} \mu \bar{\nu}_\mu$ modes [5]. This long standing issue is still unsolved despite the numerous proposed explanations.[2] In addition, there is the so-called Cabibbo-angle anomaly, a $\sim 3\sigma$ tension among the determinations of $|V_{us}|$, together with a deficit from unitarity in the first row of the CKM matrix [7].

- Tensions in observables related to the $b \to s$ transition. The branching ratios $\mathcal{B}(B \to K\mu^+\mu^-)$ and $\mathcal{B}(B_s \to \phi\mu^+\mu^-)$ are below the SM estimates. For the mode $B \to K^*\mu^+\mu^-$ a number of angular observables can be defined, which depend on q^2, the squared dilepton invariant mass [8]. For low q^2 some observables exceed the SM prediction by about 3σ [5].

- Anomalies in semileptonic decays induced by $b \to c\ell\bar{\nu}_\ell$ transition ($\ell = e, \mu, \tau$). The measured ratios of branching fractions $R(D^{(*)}) = \mathcal{B}(B \to D^{(*)}\tau\bar{\nu}_\tau)/\mathcal{B}(B \to D^{(*)}\ell\bar{\nu}_\ell)$, with $\ell = e, \mu$, exceed the SM result: the current average of BaBar, Belle and LHCb Collaborations measurements deviates by about 3σ from the SM prediction [5]. This issue challenges the SM property of lepton flavour universality.

In addition to the above tensions, a discrepancy appeared in $(g-2)_\mu$, the anomalous magnetic moment of the muon, in particular with the measurements at BNL [9] and Fermilab [10, 11]. In this observable the main uncertainty in the SM prediction is related to one of the hadronic contributions, the leading-order hadronic-vacuum-polarisation contribution (LO HVP), a nonperturbative QCD effect. A lattice QCD calculation of this contribution by the BMW Collaboration [12] differs by about 2.2σ from the one obtained by a data-driven dispersive method employing the hadronic e^+e^- cross section, used for the SM prediction in the White Paper 2020 of the $g-2$ Theory Initiative [13]. In this respect, the measurement of $\sigma(e^+e^- \to \pi^+\pi^-)$ by the CMD-3 experiment is also in tension with previous results [14]. An analysis which excludes results by data-driven dispersive methods and only uses lattice QCD determinations of the LO HVP contribution shows that measurements and SM expectations agree within the errors, which are dominated by the theory uncertainties [15]. The agreement persists for the full data set of the Muon $g-2$ Collaboration and for the combination

[1] A complete discussion is in [2].

[2] For $|V_{cb}|$ a solution based on $\mu - e$ universality violation has been proposed in [6].

JHEP12(2025)069

with all previous measurements [16]. Nevertheless, non SM contributions to $(g-2)_\mu$ still deserve to be scrutinized.

A single above mentioned deviation is not large enough to unambiguously signal NP. In general, the precision analysis is a complex task, since most observables involve SM parameters and nonperturbative quantities whose uncertainty need to be reliably assessed, as demonstrated by $(g-2)_\mu$. Methods have been proposed to get rid, to a large extent, of the errors of some SM inputs in a class of rare K and B decays [17, 18]. Taken all together the tensions could hint a BSM scenario, which however is severely constrained by the unreasonable effectiveness of the Standard Model.

A minimal extension of SM has been investigated in [1], based on the additional $\mathrm{U}(1)'$ gauge group and comprising right-handed neutrinos. The focus was on a solution found for the set of equations enabling the cancellation of the gauge anomalies induced by the new $\mathrm{U}(1)'$. In this solution the $\mathrm{U}(1)'$ charges of the fermions are generation dependent, and are expressed in terms of the SM hypercharges and of two additional rational parameters. One consequence of this assignment is a set of correlations arising among quark observables, among lepton observables and, remarkably, in the quark-lepton sectors together. Some correlations have been investigated in [1]. The conclusion was that, within the model, quark and lepton sectors mutually act to prevent large deviations from SM, justifying the small discrepancy with SM in observables where the tensions have shown up. However, the path to new physics is still viable: it relies on lepton flavour violating processes forbidden in SM, the observation of which would be a smoking gun for BSM physics. Such a kind of processes are the main topic of the present study. Within the considered framework (from now on denoted as the ABCD model), we specifically investigate possible correlations among charged lepton flavour violating (LFV) processes. We first analyse the interplay between rare beauty meson decays that conserve lepton flavour (LFC) and those exhibiting LFV. Subsequently, we explore potential correlations between processes induced by the $b \to s\ell_1^-\ell_2^+$ transition and purely leptonic LFV modes.[3]

The plan of the paper is as follows: in section 2 we describe the main features of the ABCD model, summarising the discussion in [1]. In section 3 we select the set of observables to study within the model, and identify the correlations among them to investigate. The results of the numerical analysis are presented in section 4. The conclusions are in the last section. Some details needed in the main text are included in the appendices: appendix A collects the definition of the $B \to K^*$ matrix elements of the relevant local operators in terms of form factors. Appendix B contains the expressions of the angular coefficient functions of the $B \to K^*(K\pi)\ell_1^-\ell_2^+$ fully differential decay distribution. Appendix C includes the parametrization and the values of the CKM and the Pontecorvo-Maki-Nakagawa-Sakata (PMNS) mixing matrices used in the study.

2 The ABCD model

The ABCD model is a minimal extension of the SM gauge group with an additional $\mathrm{U}(1)'$ gauge group [1]. A new neutral gauge boson Z' is predicted, with gauge coupling $g_{Z'}$. The

[3] Recent analyses of lepton flavour violating $b \to s$ modes are in [19–25].

charge associated to the $\mathrm{U}(1)'$ symmetry is named z-hypercharge. Many NP models are based on similar simple extensions, each one with specific z-hypercharge assignments [26–29]. From the experimental side, the assumption on the hypercharges determines the exclusion plots in the plane of the Z' production cross section versus the mass $M_{Z'}$.[4]

$M_{Z'}$ sets the NP scale, and it is assumed to be acquired after spontaneous breaking of the new symmetry. In the model it is not specified how the SSB happens, the only assumption is that it occurs at a much higher scale than the SM Higgs vacuum expectation value. We neglect the mixing with other neutral gauge bosons. The mass mixing vanishes at three-level if the SM Higgs is a singlet under $\mathrm{U}(1)'$. As for the kinetic mixing, it can be dealt with by recasting the gauge bosons kinetic terms in canonical form redefining the new gauge coupling [31–33]. Mixing generated by fermion loops can be neglected for processes mediated by Z' at tree-level.

Besides Z', the model comprises heavy right-handed neutrinos considered as Dirac particles. The quark sector is the same as in the SM: q_L^i are $\mathrm{SU}(2)_L$ left-handed quark doublets, u_R^i, d_R^i the right-handed singlets, $i = \{1, 2, 3\}$ is a generation index. In the lepton sector, ℓ_L^i denote the left-handed lepton doublets, ν_R^i and e_R^i the right-handed singlets. Before the electroweak SSB the Z' couplings to fermions are flavour conserving: for a generic fermion ψ the interaction Lagrangian with Z' reads

$$\mathcal{L}_{\text{int}}^{Z'}(\psi) = g_{Z'}\, z_\psi\, \bar{\psi}\, \gamma^\mu\, \psi\, Z'_\mu\,, \tag{2.1}$$

with Z'_μ the gauge boson field, $g_{Z'}$ the $\mathrm{U}(1)'$ gauge coupling and z_ψ the z-hypercharge of ψ. Hence, in terms of left- and right-handed fields $\psi_{L(R)}$ the fermion-Z' interaction Lagrangian is

$$\mathcal{L}_{\text{int}}^{Z'} = \sum_{i,j} \left[(\Delta_L^\psi)^{ij}\, \bar{\psi}_L^i\, \gamma^\mu\, \psi_L^j + (\Delta_R^\psi)^{ij}\, \bar{\psi}_R^i\, \gamma^\mu\, \psi_R^j\right] Z'_\mu\,, \tag{2.2}$$

where

$$(\Delta_{L(R)}^\psi)^{ij} = g_{Z'}\, z_{\psi_{L(R)}}\, \delta^{ij}\,. \tag{2.3}$$

After the enlargement of the gauge group, the SM remains free of gauge anomalies imposing anomaly cancellation conditions. The z-hypercharges are required to satisfy a set of six anomaly cancellation equations (ACE) [34], suitably written defining

$$z_q = \sum_{i=1}^{3} z_{q_L^i}\,, \qquad z_u = \sum_{i=1}^{3} z_{u_R^i}\,, \qquad z_d = \sum_{i=1}^{3} z_{d_R^i}\,, \tag{2.4}$$

$$z_\ell = \sum_{i=1}^{3} z_{\ell_L^i}\,, \qquad z_\nu = \sum_{i=1}^{3} z_{\nu_R^i}\,, \qquad z_e = \sum_{i=1}^{3} z_{e_R^i}\,, \tag{2.5}$$

and

$$z_f^{(2)} = \sum_{i=1,2,3} z_{f^i}^2\,, \qquad z_f^{(3)} = \sum_{i=1,2,3} z_{f^i}^3\,. \tag{2.6}$$

f^i are the fermions $f^i = q_L^i,\, u_R^i,\, d_R^i,\, \ell_L^i,\, e_R^i,\, \nu_R^i$ for the generations $i = 1, 2, 3$. In a notation where groups indicate the gauge bosons in triangular graphs, the anomaly cancellation equations read:

[4] See, e.g., the review: B.A. Dobrescu and S. Willocq, "Z'-boson searches", in [30].

1. $[\mathrm{SU}(3)_C]^2\mathrm{U}(1)'$:
$$A_{33z} = 2z_q - z_u - z_d = 0\,; \tag{2.7}$$

2. $[\mathrm{SU}(2)]^2\mathrm{U}(1)'$:
$$A_{22z} = 3z_q + z_l = 0\,; \tag{2.8}$$

3. $[\mathrm{U}(1)_Y]^2\mathrm{U}(1)'$:
$$A_{11z} = \frac{1}{6}z_q - \frac{4}{3}z_u - \frac{1}{3}z_d + \frac{1}{2}z_l - z_e = 0\,; \tag{2.9}$$

4. triangular graphs involving two gravitons and Z':
$$A_{GGz} = 3[2z_q - z_u - z_d] + 2z_l - z_e - z_\nu = 2z_l - z_e - z_\nu = 0\,, \tag{2.10}$$
(the second equation is obtained after imposing (2.7));

5. $\mathrm{U}(1)_Y[\mathrm{U}(1)']^2$:
$$A_{1zz} = [z_q^{(2)} - 2z_u^{(2)} + z_d^{(2)}] - [z_l^{(2)} - z_e^{(2)}] = 0\,; \tag{2.11}$$

6. $[\mathrm{U}(1)']^3$:
$$A_{zzz} = 3[2z_q^{(3)} - z_u^{(3)} - z_d^{(3)}] + [2z_l^{(3)} - z_\nu^{(3)} - z_e^{(3)}] = 0\,. \tag{2.12}$$

Several studies have been devoted to the rational solutions of eqs. (2.7)–(2.12) [35]. The solution proposed in the ABCD model consists in writing the z-hypercharge of each fermion f_i in terms of the SM hypercharge $y_{f_i} = y_f$ for all $i = 1, 2, 3$ (hence generation universal) plus a rational parameter ϵ_i which depends on the generation i and is the same for all fermions in the generation:
$$z_{f_i} = y_f + \epsilon_i\,. \tag{2.13}$$
This choice implies
$$z_f = \sum_{i=1}^{3} z_{f_i} = 3y_f + \epsilon\,, \tag{2.14}$$
with
$$\epsilon = \sum_{i=1}^{3} \epsilon_i\,. \tag{2.15}$$
Since the SM hypercharges y_f solve the anomaly equations, the condition for ϵ_i to solve eqs. (2.7)–(2.12) is simply [1]
$$\epsilon = \sum_{i=1}^{3} \epsilon_i = 0\,. \tag{2.16}$$

At this stage the ABCD model has four new parameters: $M_{Z'}$, g_Z, ϵ_1 and ϵ_2 (using eq. (2.16) to get rid of ϵ_3). Other parameters are involved in the fermion rotation from flavour to mass eigenstates. We denote by $\hat{V}^{\psi}_{L(R)}$ the matrix rotating left (right)-handed components of the vector of fermions $(\psi^1_{L(R)}, \psi^2_{L(R)}, \psi^3_{L(R)})$ with the same quantum numbers in the three generations, to obtain a diagonal mass matrix $(\hat{M}_\psi)_D$:

$$(\hat{M}_\psi)_D = (\hat{V}^\psi_L)^\dagger \hat{M}_\psi \hat{V}^\psi_R \,. \tag{2.17}$$

In terms of the rotated fields, eq. (2.2) reads:

$$\mathcal{L}^{Z'}_{\rm int} = \sum_{i,j} g_{Z'} \left[\bar{\psi}^i_L \gamma^\mu \, (\hat{V})^\dagger_L \hat{Z}^\psi_L \hat{V}_L \, \psi^j_L + \bar{\psi}^i_R \gamma^\mu \, (\hat{V})^\dagger_R \hat{Z}^\psi_R \hat{V}_R \, \psi^j_R\right] Z'_\mu \,, \tag{2.18}$$

where

$$\hat{Z}^\psi_{L(R)} = diag(z_{\psi^1_{L(R)}}, \, z_{\psi^2_{L(R)}}, \, z_{\psi^3_{L(R)}}) \,. \tag{2.19}$$

The Lagrangian in eq. (2.18) has the same form as in (2.2) defining

$$(\Delta^\psi_L)^{ij} = g_{Z'}[(V^\psi_L)^\dagger \hat{Z}^\psi_L V^\psi_L]^{ij} \,, \quad (\Delta^\psi_R)^{ij} = g_{Z'}[(V^\psi_R)^\dagger \hat{Z}^\psi_R V^\psi_R]^{ij} \,. \tag{2.20}$$

In SM the product $(\hat{V}^u_L)^\dagger \hat{V}^d_L$ defines the CKM matrix: $(\hat{V}^u_L)^\dagger \hat{V}^d_L = \hat{V}_{CKM}$, and it is possible to choose $\hat{V}^u_L = 1$ and $\hat{V}^d_L = \hat{V}_{CKM}$. The same choice is made in the ABCD model. The absence of right-handed charged currents and the flavour universality of the neutral currents allows also to choose $\hat{V}^u_R = 1$ in SM. This choice is not automatically justified in the ABCD model, due to the flavour nonuniversality of the Z' mediated current: the choice $\hat{V}^u_R = 1$ is retained as a model assumption. Hence, the quark sector only involves the matrices $\hat{V}_{CKM}$ and $\hat{V}^d_R$.

In the lepton sector the matrix $\hat{V}^\nu_R$ can be ignored since no phenomenological observable involving ν_R is considered. In analogy to the quark sector, the matrix $\hat{V}^\nu_L$ is set to the unit matrix and $(\hat{V}^\ell_L)^\dagger$ defines the PMNS matrix: $(\hat{V}^\ell_L)^\dagger = \hat{U}_{\rm PMNS}$. Hence, the remaining matrices in this sector are $\hat{U}_{\rm PMNS}$ and $\hat{V}^e_R$.

The parametrization of the rotation matrices can be found in [1]. Appendix C contains the choice for the parameters of the CKM and PMNS matrices. After the fermion rotations, flavour violating Z' couplings are generated, as indicated below.

- Couplings of left-handed down quarks to Z':

$$\Delta^{ij}_L = g_{Z'} \left[(2\epsilon_1 + \epsilon_2) V_{uj} V^*_{ui} + (\epsilon_1 + 2\epsilon_2) V_{cj} V^*_{ci}\right] \qquad (i \neq j) \,, \tag{2.21}$$

$$\Delta^{ii}_L = g_{Z'} \left[\frac{1}{6} + (2\epsilon_1 + \epsilon_2)|V_{ui}|^2 + (\epsilon_1 + 2\epsilon_2)|V_{ci}|^2 - \epsilon_1 - \epsilon_2\right] \,. \tag{2.22}$$

  The generation index $i = d,\, s,\, b$ is used to make the notation more transparent. V_{ui} and V_{ci} are CKM matrix elements.

- Couplings of right-handed down quarks to Z':

$$\Delta^{sd}_R = g_{Z'} \, e^{i\phi_K} \tilde{s}_{12} \, (\epsilon_1 - \epsilon_2) \,, \tag{2.23}$$

$$\Delta^{bd}_R = g_{Z'} \, e^{i\phi_d} \tilde{s}_{13} \, (2\epsilon_1 + \epsilon_2) \,, \tag{2.24}$$

$$\Delta^{bs}_R = g_{Z'} \, e^{i\phi_s} \tilde{s}_{23} \, (\epsilon_1 + 2\epsilon_2) \,, \tag{2.25}$$

$$\Delta^{ii}_R = g_{Z'} \left[-\frac{1}{3} + \epsilon_i\right] \,. \tag{2.26}$$

  The real numbers $\tilde{s}_{12}$, $\tilde{s}_{13}$, $\tilde{s}_{23}$ and the phases ϕ_K, ϕ_d, ϕ_s appear in the parametrization of the rotation matrices [1]. $(\tilde{s}_{12},\, \phi_K)$ only enter in the kaon sector, $(\tilde{s}_{13},\, \phi_d)$ only in the B_d sector, $(\tilde{s}_{23},\, \phi_s)$ only in the B_s sector.

JHEP12(2025)069

- Couplings of up-type quarks to Z':

$$\Delta_L^{ii} = g_{Z'}\left[\frac{1}{6}+\epsilon_i\right], \qquad \Delta_R^{ii} = g_{Z'}\left[\frac{2}{3}+\epsilon_i\right], \qquad (i=u,c,t)\,. \tag{2.27}$$

- Couplings of left-handed charged leptons to Z':

$$\Delta_L^{ij} = g_{Z'}\left[(2\epsilon_1+\epsilon_2)U_{i1}U_{j1}^* + (\epsilon_1+2\epsilon_2)U_{i2}U_{j2}^*\right] \qquad (i\neq j)\,, \tag{2.28}$$

$$\Delta_L^{ii} = g_{Z'}\left[-\frac{1}{2}+(2\epsilon_1+\epsilon_2)|U_{i1}|^2+(\epsilon_1+2\epsilon_2)|U_{i2}|^2-\epsilon_1-\epsilon_2\right], \tag{2.29}$$

  where $i=e,\,\mu,\,\tau$, and U_{ij} are elements of the PMNS matrix. Lepton flavour violating couplings arise for non-vanishing $\epsilon_{1,2}$.

- Couplings of right-handed charged leptons to Z':

$$\Delta_R^{\mu e} = g_{Z'}\,e^{i\phi_{12}}\tilde{t}_{12}\,(\epsilon_1-\epsilon_2)\,, \tag{2.30}$$

$$\Delta_R^{\tau e} = g_{Z'}\,e^{i\phi_{13}}\tilde{t}_{13}\,(2\epsilon_1+\epsilon_2)\,, \tag{2.31}$$

$$\Delta_R^{\tau\mu} = g_{Z'}\,e^{i\phi_{23}}\tilde{t}_{23}\,(\epsilon_1+2\epsilon_2)\,, \tag{2.32}$$

$$\Delta_R^{ii} = g_{Z'}\,[-1+\epsilon_i]\,. \tag{2.33}$$

  The real numbers $\tilde{t}_{ij}$ and the phases ϕ_{ij} are the analogous of $\tilde{s}_{ij}$ and $\phi_{K,d,s}$ in the quark sector: $(\tilde{t}_{12},\,\phi_{12})$ enter in $\mu\to e$ transitions, $(\tilde{t}_{13},\,\phi_{13})$ in $\tau\to e$ transitions, $(\tilde{t}_{23},\,\phi_{23})$ in $\tau\to\mu$ transitions. Also in this case $\epsilon_{1,2}\neq 0$ produces lepton flavour violating Z' interactions.

- Neutrino couplings to Z':

$$\Delta_L^{\nu_i\bar{\nu}_i} = g_{Z'}\left[-\frac{1}{2}+\epsilon_i\right] \qquad (i=\nu_1,\nu_2,\nu_3)\,. \tag{2.34}$$

Hence, after the fermion rotation from flavour to mass eigenstates, the free parameters in the model comprise

$$g_{Z'}\,, \qquad M_{Z'}\,, \qquad \epsilon_1\,, \qquad \epsilon_2\,, \tag{2.35}$$

with $\epsilon_{1,2}$ rational numbers, and the mixing angles and phases in the Z' couplings to right-handed fermions:

$$(\tilde{s}_{12},\,\phi_K)\,, \qquad (\tilde{s}_{13},\,\phi_d)\,, \qquad (\tilde{s}_{23},\,\phi_s) \tag{2.36}$$

for quarks, and

$$(\tilde{t}_{12},\,\phi_{12})\,, \qquad (\tilde{t}_{13},\,\phi_{13})\,, \qquad (\tilde{t}_{23},\,\phi_{23}) \tag{2.37}$$

for leptons. The Z' couplings to left-handed fermions involve the parameters of the CKM and PMNS matrices, respectively in the quark and lepton sectors.

Since the number of parameters, even in this minimal extension of the Standard Model, is not small, a strategy for their treatment needs to be envisaged. The general case where all

JHEP12(2025)069

$\tilde{s}_{ij}$ and $\tilde{t}_{ij}$ in eqs. (2.36), (2.37) are taken to be different from zero was considered, allowing for Z' couplings to all right-handed fermions [1]. This possibility, denoted as the scenario C, appeared not efficiently constrained.[5] Another strategy was adopted in two other cases. First, all $\tilde{t}_{ij}$ in (2.37) were assumed to vanish, enabling flavour violating couplings of Z' to right-handed fermions only for quarks, a case denoted as scenario B. Finally, all $\tilde{s}_{ij}$ and $\tilde{t}_{ij}$ in (2.36), (2.37) were set to zero, enabling no flavour violating couplings of Z' to right-handed fermions [1]. In this last case, the scenario A, the new parameters are only those in (2.35) together with the elements of the CKM and PMNS matrices. This most economic scenario is assumed in our study. In the following, we select a set of relevant observables, we discuss how the parameter space is constrained and the implications in a few lepton flavour conserving (LFC) and lepton flavour violating processes (LFV). Since all Z' couplings to fermions involve the two parameters $\epsilon_{1,2}$, correlations among different modes can be established: we investigate some of them, in particular the correlations between quark and lepton observables.

3 Observables

The couplings (2.21)–(2.34) show that in the ABCD model flavour changing neutral current transitions occur at tree-level through Z' exchanges, and that lepton flavour violating processes are possible. For this reason, we study the $b \to s\ell_1^- \ell_2^+$ transition, both for $\ell_1 = \ell_2$ and $\ell_1 \neq \ell_2$, focusing on the exclusive modes $B_s \to \ell_1^- \ell_2^+$, $B \to K^* \ell_1^- \ell_2^+$ and $B_s \to \phi \ell_1^- \ell_2^+$ for which a wealth of experimental information is available and some tensions are spotted. Moreover, we describe the leptonic LFV modes $\mu^- \to e^- \gamma$, $\tau^- \to \mu^- \mu^+ \mu^-$, $\mu^- \to e^- e^+ e^-$ and the $\mu^- \to e^-$ conversion in nuclei. Finally, we consider the Z' contribution to $(g-2)_\mu$.

3.1 Effective Hamiltonian for $b \to s\ell_1^- \ell_2^+$

The low-energy $\Delta B = -1$, $\Delta S = 1$ Hamiltonian governing $b \to s\ell_1^- \ell_2^+$, comprising the SM operators for $\ell_1 = \ell_2$, and operators that can be generated in BSM models with Z', has the form

$$H^{\text{eff}} = -4\,\frac{G_F}{\sqrt{2}} V_{tb} V_{ts}^* \left\{ C_1 O_1 + C_2 O_2 + \sum_{i=3,\dots,6} C_i O_i + \sum_{i=7,\dots,10} \left[C_i O_i + C_i' O_i' \right] \right\}. \tag{3.1}$$

G_F is the Fermi constant, V_{ij} are elements of the CKM matrix, and doubly Cabibbo suppressed terms proportional to $V_{ub} V_{us}^*$ are neglected.[6] The effective Hamiltonian includes the current-current operators $O_{1,2}$

$$O_1 = (\bar{c}_\alpha \gamma_\mu P_L\, b_\beta)(\bar{s}_\beta \gamma^\mu P_L\, c_\alpha)\,, \quad O_2 = (\bar{c} \gamma_\mu P_L\, b)(\bar{s} \gamma^\mu P_L\, c)\,, \tag{3.2}$$

the QCD penguin operators $O_{3,\dots,6}$

$$O_3 = (\bar{s} \gamma^\mu P_L\, b) \sum_q (\bar{q} \gamma^\mu P_L\, q)\,, \quad O_4 = (\bar{s}_\alpha \gamma^\mu P_L\, b_\beta) \sum_q (\bar{q}_\beta \gamma^\mu P_L\, q_\alpha)\,, \tag{3.3}$$

$$O_5 = (\bar{s} \gamma^\mu P_L\, b) \sum_q (\bar{q} \gamma^\mu P_R\, q)\,, \quad O_6 = (\bar{s}_\alpha \gamma^\mu P_L\, b_\beta) \sum_q (\bar{q}_\beta \gamma^\mu P_R\, q_\alpha)\,, \tag{3.4}$$

[5] In particular, the efficient constraints imposed by the $\Delta F = 2$ observables discussed in the following were not imposed.

[6] The complete basis of operators including (pseudo-)scalar and tensor operators can be found in [8].

with $P_{R,L} = \dfrac{1 \pm \gamma_5}{2}$, α,β colour indices, and the sum in (3.3)–(3.4) running over the flavours $q = u, d, s, c, b$. The other operators in (3.1) are the magnetic penguin operators

$$O_7 = \frac{e}{16\pi^2}\Big(\bar{s}\sigma^{\mu\nu}(m_s P_L + m_b P_R)\, b\Big)F_{\mu\nu}\,, \tag{3.5}$$

$$O_7' = \frac{e}{16\pi^2}\Big(\bar{s}\sigma^{\mu\nu}(m_s P_R + m_b P_L)\, b\Big)F_{\mu\nu}\,, \tag{3.6}$$

$$O_8 = \frac{g_s}{16\pi^2}\left(\bar{s}_\alpha\sigma^{\mu\nu}\left(\frac{\lambda^a}{2}\right)_{\alpha\beta}(m_s P_L + m_b P_R) b_\beta\right)G^a_{\mu\nu}\,, \tag{3.7}$$

$$O_8' = \frac{g_s}{16\pi^2}\left(\bar{s}_\alpha\sigma^{\mu\nu}\left(\frac{\lambda^a}{2}\right)_{\alpha\beta}(m_s P_R + m_b P_L) b_\beta\right)G^a_{\mu\nu}\,, \tag{3.8}$$

and the semileptonic electroweak penguin operators

$$O_9 = \frac{e^2}{16\pi^2}\Big(\bar{s}\gamma^\mu P_L\, b\Big)\,\bar{\ell}_1\gamma_\mu\ell_2\,, \qquad O_9' = \frac{e^2}{16\pi^2}\Big(\bar{s}\gamma^\mu P_R\, b\Big)\,\bar{\ell}_1\gamma_\mu\ell_2\,, \tag{3.9}$$

$$O_{10} = \frac{e^2}{16\pi^2}\Big(\bar{s}\gamma^\mu P_L\, b\Big)\,\bar{\ell}_1\gamma_\mu\gamma_5\ell_2\,, \qquad O_{10}' = \frac{e^2}{16\pi^2}\Big(\bar{s}\gamma^\mu P_R\, b\Big)\,\bar{\ell}_1\gamma_\mu\gamma_5\ell_2\,. \tag{3.10}$$

Primed operators have opposite chirality with respect to the unprimed ones. λ^a are the Gell-Mann matrices, $F_{\mu\nu}$ and $G^a_{\mu\nu}$ the electromagnetic and gluonic field strengths, e and g_s the electromagnetic and strong coupling constant. The b and s quark mass m_b and m_s are defined in the $\overline{\text{MS}}$ scheme at the scale m_b.

In SM, at the leading order in α_s the only operators to be considered are O_7 and $O_{9,10}$ with $\ell_1 = \ell_2$. At this order, O_7 is the only operator contributing to $b \to s\gamma$. The renormalization group evolution to the scale $\mu_b \simeq \mathcal{O}(m_b)$ also involves the magnetic gluon penguin operator O_8 and the operators $O_{1,\ldots 6}$. Their mixing into O_7 generates large logarithms producing a strong enhancement of the rates. The anomalous dimension matrix governing the mixing is regularization scheme dependent. One can get rid of such a dependence defining an effective coefficient $C_7^{(0)\text{eff}}(\mu_b)$ which includes contributions of $O_{1,\ldots 6}$ [36]. Non factorizable contributions to the matrix elements of O_1 and O_2 must also be taken into account. Their effects produce a further shift in the coefficient of O_7: $C_7^{\text{eff}} = 1.33\, C_7^{(0)\text{eff}}$ [37]. In this way, O_7 turns out to give the dominant contribution to $b \to s\gamma$, with the SM Wilson coefficients known at NNLO in QCD [2, 38]. O_7 contributes to $b \to s\ell_1^+\ell_2^-$ for $\ell_1 = \ell_2$, due to the photon conversion into the lepton pair.

In SM, the contribution to $b \to s\ell^+\ell^-$ comes from the operators O_9 and O_{10} and also from other operators in (3.1), in particular O_1 and O_2 due to charm re-scattering. This contribution overwhelms the contributions of the other operators in the region of q^2, the dilepton invariant mass, corresponding to the narrow charmonium resonances J/ψ, $\psi(2S)$, ... The contribution of charm re-scattering in the other intervals of q^2, the role of which has been pointed out long ago [39], has theoretical uncertainties difficult to evaluate. A possibility to account for it is to replace C_9 with $C_9^{\text{eff}} = C_9 + Y(q^2)$ [40–44], introducing a function $Y(q^2)$ which comprises the terms described in [45]. This could obscure genuine new short-distance contributions to C_9. Charm re-scattering contributions can be described through non-local form factors determined, e.g., by dispersion relations employing information from the nonleptonic modes $B \to K^*(J/\psi, \psi(2S))$ [45–48], with an uncertainty difficult to estimate [49]. In the comparison with measurements it is customary to exclude the q^2 region corresponding to the resonances J/ψ, $\psi(2S)$, which are cut in the experimental analyses to isolate the short-distance part of the q^2 spectrum [50]. Since charm re-scattering does not affect the LFV processes with $\ell_1 \neq \ell_2$, of prime interest in our study, for the $\ell^+\ell^-$ mode we also cut the resonance region and omit to include charm rescattering effects in the remaining q^2 interval.

Summarizing, we only consider the operators O_7, $O_{9,10}$ and $O'_{9,10}$ in the effective Hamiltonian (3.1) to analyse the exclusive modes $B_s \to \ell_1^- \ell_2^+$, $B \to K^* \ell_1^- \ell_2^+$ and $B_s \to \phi \ell_1^- \ell_2^+$. In SM the Wilson coefficients are flavour universal, in the ABCD extension they depend on the lepton flavour.

3.1.1 $B_s \to \ell_1^- \ell_2^+$

For the decay $B_s(p) \to \ell_1^-(k_1)\ell_2^+(k_2)$, with p and $k_{1,2}$ the particle four-momenta, a single hadronic quantity is required, the decay constant f_{B_s} defined by

$$\langle 0|\bar{s}\gamma_\mu\gamma_5 b|B_s(p)\rangle = i\, f_{B_s} p_\mu\,. \tag{3.11}$$

The branching fraction is given by

$$\begin{aligned}\bar{\mathcal{B}}(B_s \to \ell_1^- \ell_2^+) = \frac{\tau_{B_s}}{(1-y_s)} & \frac{G_F^2 \alpha^2 |\lambda_{ts}^*|^2 f_{B_s}^2}{64\pi^3 m_{B_s}^3} \lambda^{1/2}(m_{B_s}^2, m_{\ell_1}^2, m_{\ell_2}^2) \\ & \times \Big\{ |C_9 - C_9'|^2 (m_{\ell_1} - m_{\ell_2})^2 \left[m_{B_s}^2 - (m_{\ell_1} + m_{\ell_2})^2\right] \\ & + |C_{10} - C_{10}'|^2 (m_{\ell_1} + m_{\ell_2})^2 \left[m_{B_s}^2 - (m_{\ell_1} - m_{\ell_2})^2\right] \Big\}\,, \end{aligned} \tag{3.12}$$

with $\lambda_{ts}^* = V_{tb}V_{ts}^*$, $\lambda(x,y,z) = x^2 + y^2 + z^2 - 2xy - 2xz - 2yz$ the Källen function, τ_{B_s} the average B_s lifetime. The notation $\bar{\mathcal{B}}$ indicates that the effects of the $B_s - \bar{B}_s$ oscillations are taken into account through the factor $1/(1-y_s)$ [51], with $y_s = 0.061 \pm 0.009$ [52]. In SM with $\ell_1 = \ell_2$ eq. (3.12) shows that only the operator O_{10} contributes to this decay.

3.1.2 $\bar{B}^0 \to \bar{K}^{*0} \ell_1^- \ell_2^+$ and $B_s \to \phi \ell_1^- \ell_2^+$

Let us consider $\bar{B}^0(p) \to \bar{K}^{*0}(p', \epsilon)\ell_1^-(k_1)\ell_2^+(k_2)$ (the description of $B_s \to \phi\ell_1^-\ell_2^+$ is analogous). ϵ is the K^* polarization four-vector, $q = k_1 + k_2$. The local form factors parametrising the matrix elements of the operators in (3.1) are defined in appendix A. Considering the subsequent $K^* \to K\pi$ transition and the kinematics in figure 1, the fully differential decay distribution in q^2 and in the angles θ_ℓ, θ_{K^*}, ϕ has the expression

$$\frac{d^4\Gamma(\bar{B}^0 \to \bar{K}^{*0}(K\pi)\ell_1^-\ell_2^+)}{dq^2\, d\cos\theta_\ell\, d\cos\theta_{K^*}\, d\phi} = \frac{9}{32\pi} I(q^2, \theta_\ell, \theta_{K^*}, \phi)\,. \tag{3.13}$$

JHEP12(2025)069

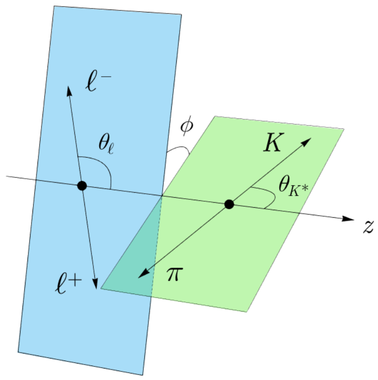

Figure 1. Kinematics of the decay $\bar{B}^0 \to \bar{K}^{*0}(K\pi)\ell_1^-\ell_2^+$.

The function $I(q^2, \theta_\ell, \theta_{K^*}, \phi)$ can be written in terms of angular coefficient functions $I_i^{(a)}(q^2)$ using the decomposition [8]

$$\begin{aligned} I(q^2,\theta_\ell,\theta_{K^*},\phi) = {} & I_1^s(q^2)\sin^2\theta_{K^*} + I_1^c(q^2)\cos^2\theta_{K^*} + [I_2^s(q^2)\sin^2\theta_{K^*} + I_2^c(q^2)\cos^2\theta_{K^*}]\cos 2\theta_\ell \\ & + I_3(q^2)\sin^2\theta_{K^*}\sin^2\theta_\ell\cos 2\phi + I_4(q^2)\sin 2\theta_{K^*}\sin 2\theta_\ell\cos\phi \\ & + I_5(q^2)\sin 2\theta_{K^*}\sin\theta_\ell\cos\phi \\ & + [I_6^s(q^2)\sin^2\theta_{K^*} + I_6^c(q^2)\cos^2\theta_{K^*}]\cos\theta_\ell + I_7(q^2)\sin 2\theta_{K^*}\sin\theta_\ell\sin\phi \\ & + I_8(q^2)\sin 2\theta_{K^*}\sin 2\theta_\ell\sin\phi + I_9(q^2)\sin^2\theta_{K^*}\sin^2\theta_\ell\sin 2\phi . \end{aligned} \tag{3.14}$$

$I_i^{(a)}$ depend on the Wilson coefficients in (3.1), hence they probe the SM. They also depend on the hadronic form factors. Their expressions in terms of amplitudes for the various K^* polarizations and lepton chiralities are in appendix B. Integration over the three angles ϕ, θ_ℓ and θ_{K^*} provides the q^2 spectrum:

$$\frac{d\Gamma}{dq^2} = \frac{1}{4}\Big[6I_1^s(q^2) + 3I_1^c(q^2) - 2I_2^s(q^2) - I_2^c(q^2)\Big], \tag{3.15}$$

further integration over the physical range $q^2 \in [(m_{\ell_1} + m_{\ell_2})^2, (m_B - m_{K^*})^2]$ gives the decay width.

The hadronic uncertainties can obscure the sensitivity to NP, therefore it is convenient to define observables in which such uncertainties to a large extent cancel out. A possibility is to consider the distribution analogous to (3.14) for the CP conjugate decay mode, with angular coefficient functions $\bar{I}_i^{(a)}$, and define CP-even and CP-odd quantities:

$$S_i^{(a)}(q^2) = \Big(I_i^{(a)}(q^2) + \bar{I}_i^{(a)}(q^2)\Big) \Big/ \Big(d\Gamma/dq^2 + d\bar{\Gamma}/dq^2\Big), \tag{3.16}$$

$$A_i^{(a)}(q^2) = \Big(I_i^{(a)}(q^2) - \bar{I}_i^{(a)}(q^2)\Big) \Big/ \Big(d\Gamma/dq^2 + d\bar{\Gamma}/dq^2\Big). \tag{3.17}$$

$d\bar{\Gamma}/dq^2$ is the distribution analogous to (3.15) for the CP conjugated mode. Starting from such expressions, several observables can be built. In SM, S_7, S_8 and S_9 are tiny.

We focus on the forward-backward asymmetry with respect to the direction of the emitted lepton

$$A_{FB}(q^2) = \frac{3}{8}[2S_6^s(q^2) + S_6^c(q^2)], \tag{3.18}$$

JHEP12(2025)069

on the fraction of longitudinally and transversely polarized K^*

$$F_L(q^2) = -S_2^c(q^2)\,, \qquad F_T(q^2) = 1 - F_L(q^2)\,, \tag{3.19}$$

and on the angular P-observables [53]

$$\begin{aligned} P_1(q^2) &= \frac{2}{F_T(q^2)} S_3(q^2)\,, \quad P_2(q^2) = \frac{1}{2F_T(q^2)} S_{6s}(q^2)\,, \quad P_3(q^2) = -\frac{1}{F_T(q^2)} S_9(q^2)\,, \\ P'_{4,5,6}(q^2) &= \frac{1}{\sqrt{F_L(q^2)\, F_T(q^2)}} S_{4,5,7}(q^2)\,. \end{aligned} \tag{3.20}$$

The forward-backward asymmetry is recognised to be sensitive to NP, in particular because in SM it changes sign in the physical q^2 range [44, 54–57], with the zero q_0^2 determined by

$$\mathrm{Re}[C_9] + \frac{m_b}{q_0^2}\mathrm{Re}[C_7]\left[(m_B + m_{K^*})\frac{T_1(q_0^2)}{V(q_0^2)} + (m_B - m_{K^*})\frac{T_2(q_0^2)}{A_1(q_0^2)}\right] = 0\,. \tag{3.21}$$

A model independent prediction for q_0^2 is obtained in the large energy limit of K^*, due to spin symmetry relations among the form factors [58]

$$\frac{T_1(E)}{V(E)} = \frac{m_B}{m_B + m_{K^*}}\,, \qquad \frac{T_2(E)}{A_1(E)} = \frac{(m_B + m_{K^*})}{m_B}\,, \tag{3.22}$$

where E is the K^* energy in the B rest frame.[7] Since $m_{K^*}^2 \ll m_B^2$, eqs. (3.21), (3.22) give

$$\mathrm{Re}\,[C_9] q_0^2 + 2 m_B m_b \mathrm{Re}[C_7] = 0\,. \tag{3.23}$$

Deviations from this result would signal non SM operators in the effective Hamiltonian or/and modified values of the Wilson coefficients. Another observable

$$A_T^{(2)}(q^2) = \frac{2S_3(q^2)}{1 - F_L(q^2)} \tag{3.24}$$

is sensitive to the virtual photon polarization [60, 61], which in SM is mainly left-handed, the right-handed polarization being suppressed by m_s/m_b. Deviations are expected in scenarios where the photon can also be right-handed, an effect encoded in the operator O_7', which is not generated in the scenario A of the ABCD model.

3.2 LFV lepton decays

In this section we examine the contribution of Z' to LFV leptonic modes. We begin with the processes $\mu^- \to e^-\gamma$, $\tau^- \to \mu^-\mu^+\mu^-$ and $\mu^- \to e^-e^+e^-$. In absence of neutrino oscillations such processes do not occur in SM. In a minimal extension allowing for neutrino masses and mixing, they can occur at rates much smaller than the present experimental upper bounds discussed below. We then turn to the $\mu^- \to e^-$ conversion in nuclei.

[7]The relations (3.22) are broken by hard gluon corrections to the weak vertex and by hard spectator interactions [59].

- $\mu^- \to e^-\gamma$

  In a version of the SM extended with the seesaw mechanism to describe massive neutrinos this process can occur through a penguin diagram with internal W and oscillating neutrinos. The photon is emitted by W. If there is a Z' with LFV couplings, other penguin diagrams contribute, with Z' and a charged lepton in the loop. The branching fraction is [62]

$$\mathcal{B}(\mu \to e\gamma) = \frac{3(4\pi)^3\alpha}{4G_F^2}\left[|A^M_{e\mu}|^2 + |A^E_{e\mu}|^2\right], \tag{3.25}$$

  where

$$A^M_{e\mu} = -\frac{1}{96\pi^2 M^2_{Z'}}\sum_{f=e,\mu,\tau}\left[\Delta^{fe*}_V\Delta^{f\mu}_V\left(1-3\frac{m_f}{m_\mu}\right) + \Delta^{fe*}_A\Delta^{f\mu}_A\left(1+3\frac{m_f}{m_\mu}\right)\right], \tag{3.26}$$

$$A^E_{e\mu} = \frac{i}{96\pi^2 M^2_{Z'}}\sum_{f=e,\mu,\tau}\left[\Delta^{fe*}_A\Delta^{f\mu}_V\left(1-3\frac{m_f}{m_\mu}\right) + \Delta^{fe*}_V\Delta^{f\mu}_A\left(1+3\frac{m_f}{m_\mu}\right)\right], \tag{3.27}$$

  and Δ^{ij}_V and Δ^{ij}_A defined as

$$\Delta^{ij}_V = \Delta^{ij}_R + \Delta^{ij}_L\,, \qquad \Delta^{ij}_A = \Delta^{ij}_R - \Delta^{ij}_L\,. \tag{3.28}$$

  The sum in (3.26), (3.27) is over the charged leptons in the loop.

- $\ell_j \to \ell_i\bar{\ell}_l\ell_k$

  In the seesaw extended SM these modes are also described by loop diagrams, either penguins or boxes. In the ABCD model a tree-level diagram contributes with Z' as mediator. The generated operators and their Wilson coefficients are

$$[O_{VXY}]^{ij}_{kl} = (\bar{\psi}_i\gamma^\mu P_X\psi_j)(\bar{\psi}_k\gamma_\mu P_Y\psi_l)\,, \qquad [C_{VXY}]^{ij}_{kl} = \frac{\Delta^{ij}_X\Delta^{kl}_Y}{M^2_{Z'}}\,, \tag{3.29}$$

  with $X, Y = L, R$. The branching fraction of $\tau^- \to \mu^-\mu^+\mu^-$ is given by [1]:

$$\mathcal{B}(\tau^- \to \mu^-\mu^+\mu^-) = \frac{m_\tau^5}{1536\pi^3\Gamma_\tau}\left[2|C_{VLL}|^2 + 2|C_{VRR}|^2 + |C_{VLR}|^2 + |C_{VRL}|^2\right]^{\mu\tau}_{\mu\mu}, \tag{3.30}$$

  with Γ_τ the τ full decay width and a 1/2 factor due to the identical leptons in the final state. Analogous expressions hold for $\tau^- \to e^-e^+e^-$ and $\mu^- \to e^-e^+e^-$.

- $\mu^- - e^-$ conversion in nuclei

  The $\mu^- - e^-$ conversion in a nucleus of atomic number Z and mass number A is the process

$$\mu^- + (A, Z) \to e^- + (A, Z)\,. \tag{3.31}$$

  The transition rate $\Gamma(\mu \to e)$ in the ABCD model is obtained considering the dominant tree-level Z' contributions inducing four-fermion operators, and assuming that the conversion leaves the nucleus in its ground state [63, 64]:

$$\Gamma(\mu^- \to e^-) = \frac{\alpha^3}{16\pi^2}\frac{Z_{\text{eff}}^4}{Z}|F(q)|^2 \, \frac{m_\mu^5}{M_{Z'}^4}\left[|\Delta_L^{\mu e}(Z')|^2 + |\Delta_R^{\mu e}(Z')|^2\right]$$
$$\times \left|(2Z+N)\Delta_V^{uu}(Z') + (Z+2N)\Delta_V^{dd}(Z')\right|^2 . \tag{3.32}$$

$\Delta_V^{ij}(Z')$ are in (3.28). $N = A - Z$ is the number of neutrons in the nucleus, Z_{eff} is an effective parameter and $F(q^2)$ the nuclear form factor. The observable to investigate is the branching fraction defined as

$$\mathcal{B}(\mu^- \to e^-) = \frac{\Gamma(\mu^- \to e^-)}{\Gamma_{\text{capt}}} , \tag{3.33}$$

which involves the muon capture rate Γ_{capt} in the nucleus. The upper bound for $\mathcal{B}(\mu \to e)$ in ${}^{48}_{22}\text{Ti}$ established by the SINDRUM II experiment at PSI [65] is

$$\mathcal{B}(\mu^- \to e^-) \le 4.3 \times 10^{-12} \quad (\text{at } 90\% \text{ C.L.}) . \tag{3.34}$$

For ${}^{48}_{22}\text{Ti}$ the values of the relevant parameters are $Z_{\text{eff}} = 17.6$ and $F(q^2 \simeq -m_\mu^2) \simeq 0.54$ [66], with the muon capture rate $\Gamma_{\text{capt}} \simeq (2.590 \pm 0.012) \times 10^6 \text{ s}^{-1}$ [67]. This is the case considered in our analysis. An upper bound has been established by the SINDRUM II Collaboration also for the gold target: $\mathcal{B}(\mu^-\text{Au} \to e^-\text{Au}) \le 7 \times 10^{-13}$ [68]. Its analysis requires a different set of nuclear input parameters, that can be inferred from [64, 67]. The results of our study do not change if the experimental bound and the parameters for the gold target are used.

3.3 $(g-2)_{e,\mu}$

The Z' contribution to the muon anomalous magnetic moment $a_\mu = \dfrac{(g-2)_\mu}{2}$ has been obtained in [1] using the general formulae in [62]:

$$\Delta a_\mu \simeq -\frac{1}{16\pi^2}\frac{m_\mu^2}{M_{Z'}^2}\sum_{f=e,\mu,\tau}\left[\left|\Delta_V^{f\mu}\right|^2\left(\frac{2}{3} - \frac{m_f}{m_\mu}\right) + \left|\Delta_A^{f\mu}\right|^2\left(\frac{2}{3} + \frac{m_f}{m_\mu}\right)\right] . \tag{3.35}$$

$\Delta_{V(A)}^{ij}$ are defined in (3.28), and the sum is over internal charged leptons in the loop. For the electron, Δa_e is obtained replacing μ by e in (3.35).

4 Numerical analysis, results and correlations

As mentioned in section 2, in the ABCD model various scenarios have been considered for the Z' couplings to fermions [1]. One of them, the scenario A, consists in assuming flavour violating couplings of Z' only with left-handed fermions, obtained setting to zero the parameters in (2.36)–(2.37). The present study is based on this minimal scenario.

The list of the parameters consists of the four entries in (2.35) and of the parameters of the CKM and PMNS matrices. The coupling $g_{Z'}$ is varied in the range $g_{Z'} \in [0.01, 0.1]$, and two cases are considered for the Z' mass, $M_{Z'} = 1\,\text{TeV}$ and $M_{Z'} = 3\,\text{TeV}$. The four

JHEP12(2025)069

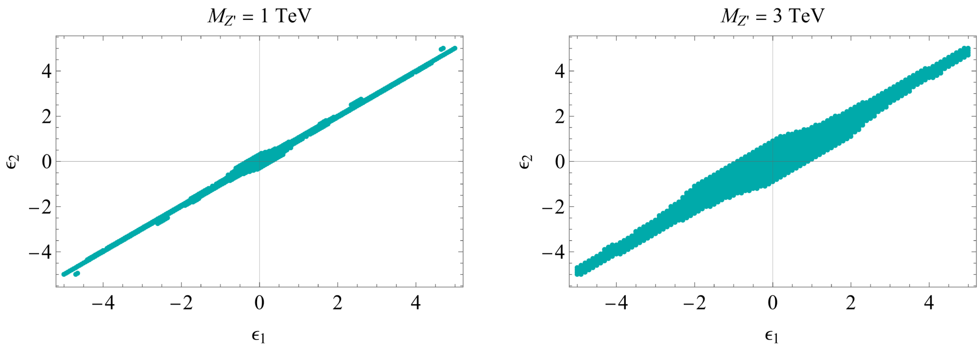

Figure 2. Allowed region in the (ϵ_1, ϵ_2) plane after imposing $\Delta F = 2$ constraints, for $M_{Z'} = 1\,\text{TeV}$ (left panel) and $M_{Z'} = 3\,\text{TeV}$ (right panel).

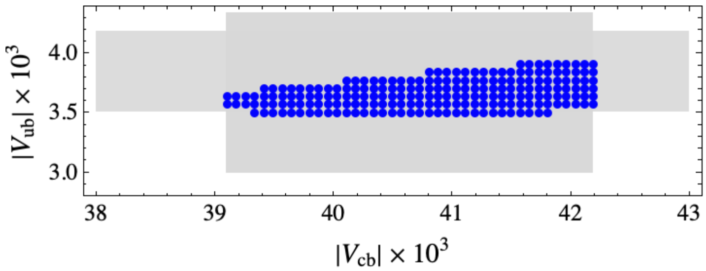

Figure 3. Allowed region in the $|V_{cb}|$, $|V_{ub}|$ plane after imposing the $\Delta F = 2$ constraints (dark blue points) for $M_{Z'} = 1\,\text{TeV}$ and $3\,\text{TeV}$. The light shaded area corresponds to the ranges (4.1).

independent parameters of the CKM matrix are taken as V_{us}, γ, $|V_{cb}|$ and $|V_{ub}|$, see appendix C. The strategy adopted in the present study consists in varying $|V_{cb}|$ and $|V_{ub}|$ in the ranges determined by the exclusive and inclusive measurements,

$$|V_{cb}| \in \left[|V_{cb}|_{\text{exc}},\, |V_{cb}|_{\text{inc}}\right], \qquad |V_{ub}| \in \left[|V_{ub}|_{\text{exc}},\, |V_{ub}|_{\text{inc}}\right], \tag{4.1}$$

instead of choosing some preferred value. All values are quoted in the appendix C, together with the parameters of the PMNS matrix. The parameter space (ϵ_1, ϵ_2) is constrained using $\Delta F = 2$ observables, modifying the SM expressions to account for the Z' contribution. Such observables are the mass differences ΔM_d, ΔM_s, ΔM_K between the neutral mesons B_d, B_s and kaons, the CP asymmetries $S_{\psi K_s}$, $S_{\psi\phi}$ and the CP violating parameter in the kaon sector ϵ_K. All quantities are related to the neutral meson $M - \bar{M}$ mixing ($M = K^0$, $B_{d,s}$), which in SM only appears at the one-loop level due to box diagrams mediated by internal up-type quark exchanges [2]. In the B_d and B_s cases the dominant contribution is by the intermediate top quark, for kaon the charm exchange must also be taken into account. The SM result depends on the Inami-Lim function $S_0(x_t)$ for $B_{d,s}$, and on $S_0(x_c, x_t)$ for kaon. Moreover, the GIM mechanism allows to get rid of mass independent terms. In the ABCD model, neutral meson mixings receive a tree-level contribution from the Z' exchange. This leads to a modification of the Inami-Lim function, $S(M) = S_0 + \Delta S(M)$ for $M = K^0$, $B_{d,s}$, with $\Delta S(M)$ given in [69]. The ABCD parameters enter in $\Delta S(M)$ through the Z' couplings to fermions, which allows to effectively constrain the parameter space by the precise experimental values for such observables. We proceed as in [1]: ΔM_d, ΔM_s and the CP asymmetries $S_{J\psi K_s}$, $S_{\phi\psi}$

JHEP12(2025)069

are required to stay in a range around 5% of the central value of the experimental datum, ΔM_K is required to lie within 25% of the SM value, accounting for possible long-distance contributions, and ϵ_K in the range $\epsilon_K \in [2.0, 2.5] \times 10^{-3}$.

The allowed regions in the (ϵ_1, ϵ_2) plane are displayed in figure 2 for the two values of $M_{Z'}$. The regions are broader than those found in [1], a consequence of scanning $|V_{cb}|$ and $|V_{ub}|$ in the exclusive-inclusive ranges instead of choosing a preferred value.

A remarkable result, shown in figure 3, is that the scan over the parameter space subject to the $\Delta F = 2$ constraints does not yield any configuration with $|V_{ub}|$ equal to the inclusive determination. The largest obtained value is $|V_{ub}| = 3.92 \times 10^{-3}$ (within the resolution set by the scan step), which indicates a preference for smaller values. This agrees with the conclusions of the discussion in [70] on the sensitivity of $\Delta F = 2$ observables to the precise values of the CKM parameters.

After having imposed the $\Delta F = 2$ constraints, we first look for deviations in lepton-flavour-conserving (LFC) B and B_s decays and for the correlations with the corresponding lepton-flavour-violating (LFV) modes. The LFC processes provide non-trivial constraints on the LFV ones.

We then study the correlations with purely leptonic LFV processes, in particular with $\tau^- \to \mu^-\mu^+\mu^-$, $\mu^- \to e^-\gamma$, $\mu^- \to e^-e^+e^-$ and $\mu^- \to e^-$ conversion in nuclei, obtaining that the experimental upper bounds on such purely leptonic channels play a hierarchical role in constraining the branching ratios of LFV B and B_s decays. The bound on $\tau^- \to \mu^-\mu^+\mu^-$ does not impose significant restrictions, whereas the other three channels set progressively more stringent limits. The correlations with $\tau^- \to \mu^-\mu^+\mu^-$, $\mu^- \to e^-\gamma$ allow branching ratios for the LFV beauty meson decays of $\mathcal{O}(10^{-9})$. Including constraints from $\mu^- \to e^-e^+e^-$ and $\mu^- \to e^-$ conversion in nuclei, the branching fractions are pushed down to $\mathcal{O}(10^{-11})$ and $\mathcal{O}(10^{-13})$, as discussed below.

4.1 $b \to s\ell_1^+\ell_2^-$

In SM where only $\ell_1 = \ell_2$ is allowed, the values of the Wilson coefficients of the operators O_7 and $O_{9,10}$ in the low-energy Hamiltonian (3.1) read [71]:

$$C_7^{\text{eff}}(m_b) = -0.450\,, \qquad C_9(m_b) = 4.273\,, \qquad C_{10}(m_b) = -4.166\,, \tag{4.2}$$

with C_7^{eff} defined in section 3.1. Efforts have been spent in global analyses to identify the coefficients deviating from the SM value, and to which extent, to reproduce the experimental data [72–75]. In the scenario A of the ABCD model there are no contributions to the coefficients of the primed operators in (3.1). The Z' contribution to C_7 is negligible with respect to SM [69]. The contributions to C_9 and C_{10} for $M_{Z'} = 1\,\text{TeV}$ and $3\,\text{TeV}$ are displayed in figures 4 and 5, where each point corresponds to a pair real/imaginary part of the coefficients computed for the same values of the parameters. The contributions to the real parts can be sizeable, up to $\pm 10\%$ of the SM values. Imaginary parts of $\mathcal{O}(10^{-4})$ are generated, originating from the phases of the CKM and PMNS matrices. The correlations between the real parts of the coefficients are displayed in the plots in figure 6 for $M_{Z'} = 1$ and $3\,\text{TeV}$.

The values of C_9^{NP} and C_{10}^{NP} obtained for the lepton flavour violating modes $b \to s\mu^-\tau^+$, together with their correlation, are displayed in the same figures 4, 5 and 6. The anticorrelation

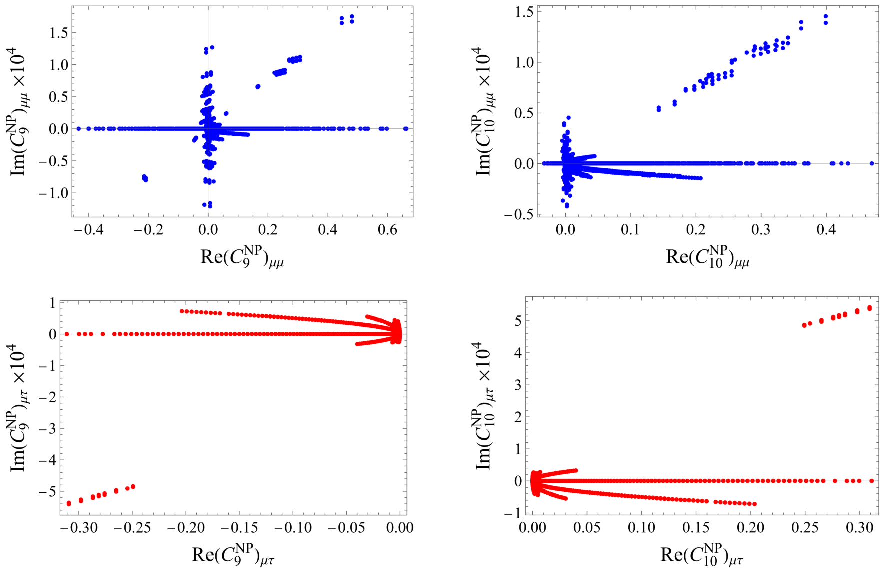

Figure 4. Correlation between real and imaginary parts of the Z' contributions to the Wilson coefficients C_9 (left panels) and C_{10} (right panels) for the LFC $b \to s\mu^-\mu^+$ (top panels) and LFV $b \to s\mu^-\tau^+$ transition (bottom panels). The Z' mass is set to $M_{Z'} = 1\,\mathrm{TeV}$.

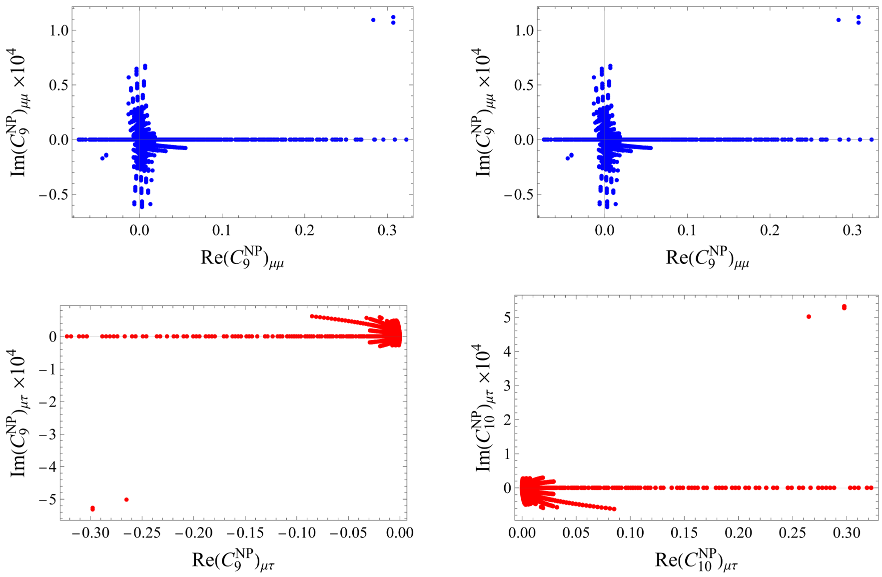

Figure 5. Correlation between real and imaginary parts of the Z' contributions to the Wilson coefficients C_9 and C_{10} as in figure 4, for $M_{Z'} = 3\,\mathrm{TeV}$.

JHEP12(2025)069

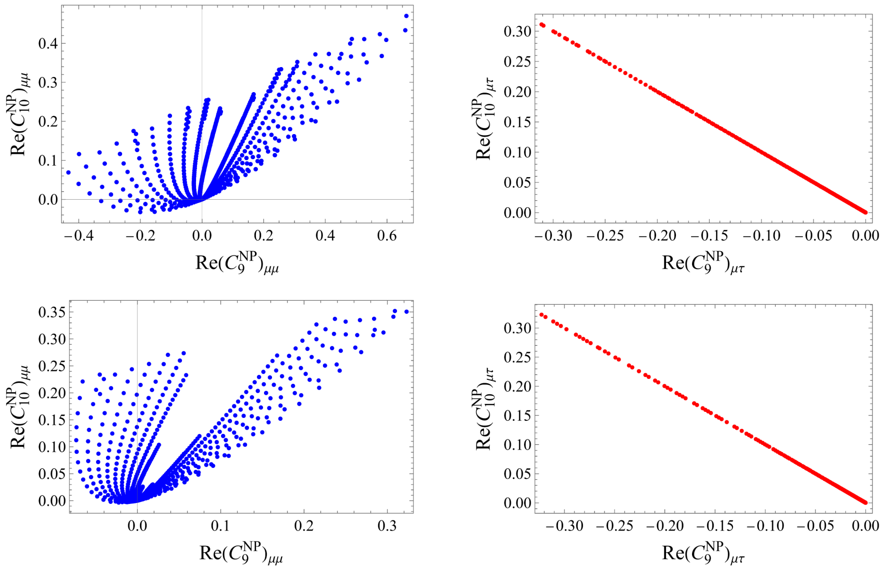

Figure 6. Correlation between the real parts of the Z' contributions to Wilson coefficients $(C_9)_{\mu\mu}$ and $(C_{10})_{\mu\mu}$ (left panels) and $(C_9)_{\mu\tau}$ and $(C_{10})_{\mu\tau}$ (right panels) for $M_{Z'} = 1\,\mathrm{TeV}$ (top panels) and for $M_{Z'} = 3\,\mathrm{TeV}$(bottom panels).

between $(C_9^{NP})_{\mu\tau}$ and $(C_{10}^{NP})_{\mu\tau}$ is a feature of the scenario A of the ABCD model. Indeed, the expressions of the coefficients are

$$(C_9^{NP})_{\ell_1\ell_2} = -\frac{1}{g_{\mathrm{SM}}^2 s_W^2 M_{Z'}^2 \lambda_{ts}^*} (\Delta_L^{bs})^* \Delta_V^{\ell_1\ell_2} \,, \qquad (C_{10}^{NP})_{\ell_1\ell_2} = -\frac{1}{g_{\mathrm{SM}}^2 s_W^2 M_{Z'}^2 \lambda_{ts}^*} (\Delta_L^{bs})^* \Delta_A^{\ell_1\ell_2} \,, \tag{4.3}$$

with $g_{\mathrm{SM}}^2 = \dfrac{4G_F}{\sqrt{2}} \dfrac{e^2}{8\pi^2 s_W^2}$, s_W the sine of the Weinberg angle, and $\Delta_{V(A)}^{\ell_1\ell_2}$ defined in (3.28). In the scenario A where the Z' flavour violating couplings to right-handed fermions vanish, we have $\Delta_V^{\ell_1\ell_2} = -\Delta_A^{\ell_1\ell_2}$ for $\ell_1 \neq \ell_2$.

4.1.1 Exclusive lepton flavour conserving $b \to s\ell^+\ell^-$ modes

The simplest process induced by $b \to s\ell^+\ell^-$ is the purely leptonic B_s decay, that we analyse using $f_{B_s} = 230.3 \pm 1.3\,\mathrm{MeV}$ [5]. Figure 7 shows the branching fractions $\bar{\mathcal{B}}(B_s \to \mu^+\mu^-)$ and $\bar{\mathcal{B}}(B_s \to \tau^+\tau^-)$ for $M_{Z'} = 1$ TeV and 3 TeV. In SM we find $\bar{\mathcal{B}}(B_s \to \mu^+\mu^-) = (3.65 \pm 0.10) \times 10^{-9}\,(|\lambda_{ts}^*|/0.04)^2$ and $\bar{\mathcal{B}}(B_s \to \tau^+\tau^-) = (7.70 \pm 0.10) \times 10^{-7}\,(|\lambda_{ts}^*|/0.04)^2$. The experimental world average $\bar{\mathcal{B}}(B_s \to \mu^+\mu^-)_{\mathrm{exp}} = (3.34 \pm 0.27) \times 10^{-9}$ [30] is indicated in figure 7. The results in the ABCD model encompass the experimental range. Moreover, requiring that $\bar{\mathcal{B}}(B_s \to \mu^+\mu^-)$ agrees with experiment, $\bar{\mathcal{B}}(B_s \to \tau^+\tau^-) = (8.2 \pm 0.5) \times 10^{-7}$ is predicted for $M_{Z'} = 1$ TeV, and $\bar{\mathcal{B}}(B_s \to \tau^+\tau^-) = (8.2 \pm 0.8) \times 10^{-7}$ for $M_{Z'} = 3\,\mathrm{TeV}$. The correlation between the two purely leptonic modes is shown in the figure, where each point corresponds to the branching fractions of $B_s \to \mu^+\mu^-$ and $B_s \to \tau^+\tau^-$ computed with the same set of parameters. Figure 7 shows that when $\bar{\mathcal{B}}(B_s \to \mu^+\mu^-)$ is predicted within its experimental range, the branching ratio $\bar{\mathcal{B}}(B_s \to \tau^+\tau^-)$ is also constrained. This feature emerges from the numerical scan, and can be understood from the analytic structure of the amplitudes in

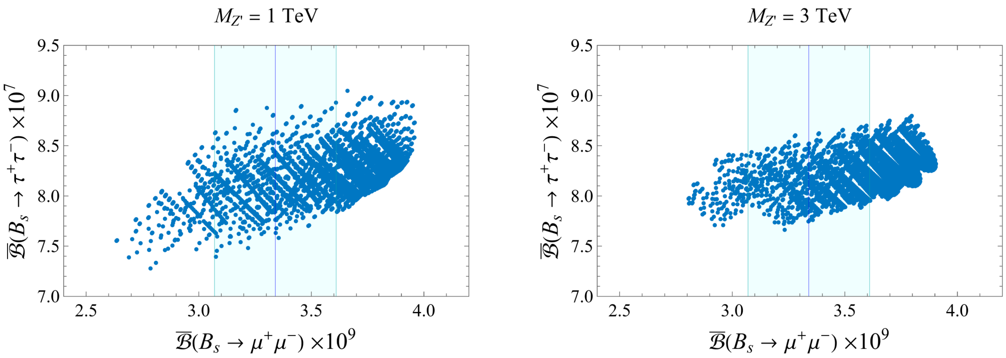

Figure 7. Correlation between $\bar{\mathcal{B}}(B_s \to \mu^+\mu^-)$ and $\bar{\mathcal{B}}(B_s \to \tau^+\tau^-)$ for $M_{Z'} = 1\,\text{TeV}$ (left) and $M_{Z'} = 3\,\text{TeV}$ (right panel). The shaded region corresponds to the experimental world average for $\bar{\mathcal{B}}(B_s \to \mu^+\mu^-)$ [30].

scenario A. Indeed, eq. (3.12) shows that both branching ratios are proportional to $|C_{10}|^2$,

$$\bar{\mathcal{B}}(B_s \to \ell^+\ell^-) = K_\ell \times |C_{10}|^2 = K_\ell \times \left|C_{10}^{\rm SM} + (C_{10}^{NP})_{\ell\ell}\right|^2 , \tag{4.4}$$

with K_ℓ a numerical factor different for $\ell = \mu$ and $\ell = \tau$. From eq. (4.3) one observes that $(C_{10}^{NP})_{\mu\mu}$ and $(C_{10}^{NP})_{\tau\tau}$ differ for the term $\Delta_A^{\ell\ell}$ that depends on the scanned parameters. Using eq. (2.28) one finds

$$(C_{10}^{NP})_{\tau\tau} \simeq (C_{10}^{NP})_{\mu\mu} + f(g_Z, \epsilon_1, \epsilon_2) , \tag{4.5}$$

where f depends on the scanned parameters. Hence, one writes

$$\bar{\mathcal{B}}(B_s \to \tau^+\tau^-) \simeq \frac{\lambda^{1/2}(m_{B_s}^2, m_\tau^2, m_\tau^2)}{\lambda^{1/2}(m_{B_s}^2, m_\mu^2, m_\mu^2)} \left[\bar{\mathcal{B}}(B_s \to \mu^+\mu^-) + \tilde{f}(g_Z, \epsilon_1, \epsilon_2)\right] , \tag{4.6}$$

where $\tilde{f}(g_Z, \epsilon_1, \epsilon_2)$ denotes the terms taking into account the function f in eq. (4.5). This relation shows that the experimental bound on $\bar{\mathcal{B}}(B_s \to \mu^+\mu^-)$ also limits $\bar{\mathcal{B}}(B_s \to \tau^+\tau^-)$.

For the lepton flavour conserving modes $B \to K^*\ell^+\ell^-$, with $\ell = \mu, \tau$, we use the local form factors determined in [76] and described in appendix A. Figure 8 shows the correlation between the branching fractions $\mathcal{B}(\bar{B}^0 \to \bar{K}^{*0}\mu^+\mu^-)$ and $\mathcal{B}(\bar{B}^0 \to \bar{K}^{*0}\tau^+\tau^-)$. The vertical band corresponds to the measurement $\mathcal{B}(\bar{B}^0 \to \bar{K}^{*0}\mu^+\mu^-)_{\rm exp} = (9.4 \pm 0.5) \times 10^{-7}$ [30]. In the case of $B \to K^*\tau^+\tau^-$ only an upper limit is known: $\mathcal{B}(\bar{B}^0 \to \bar{K}^{*0}\tau^+\tau^-) < 3.1 \times 10^{-3}$. In the ABCD model the result for $\mathcal{B}(\bar{B}^0 \to K^{*0}\mu^+\mu^-)$ encompasses the experimental interval. Requiring that it lies in the measured range, the predictions $\mathcal{B}(\bar{B}^0 \to \bar{K}^{*0}\tau^+\tau^-) = (8.6 \pm 1.3) \times 10^{-8}$ and $\mathcal{B}(\bar{B}^0 \to \bar{K}^{*0}\tau^+\tau^-) = (8.6 \pm 0.9) \times 10^{-8}$ are obtained for $M_{Z'} = 1$ and $3\,\text{TeV}$, respectively. For the SM we have: $\mathcal{B}(\bar{B}^0 \to \bar{K}^{*0}\mu^+\mu^-) = (9.6 \pm 2.0) \times 10^{-7}\,(|\lambda_{ts}^*|/0.04)^2$ and $\mathcal{B}(\bar{B}^0 \to \bar{K}^{*0}\tau^+\tau^-) = (9.2 \pm 2.0) \times 10^{-8}\,(|\lambda_{ts}^*|/0.04)^2$.

The $B \to K^*(K\pi)\mu^+\mu^-$ angular distribution has been experimentally studied in details [77–84], finding a deviation from SM predictions in some angular P-observables defined in (3.20) [50, 85–90]. In the analysis of the ABCD model predictions, to make the comparison with SM more transparent, we define the rescaled angular coefficient functions $\tilde{I}_i = I_i/|\lambda_{ts}^*|^2$, with $i = 1s, \ldots 6s$, and display them in figures 9, 10 for $\ell = \mu$ and $\ell = \tau$, setting $M_{Z'} = 1\,\text{TeV}$

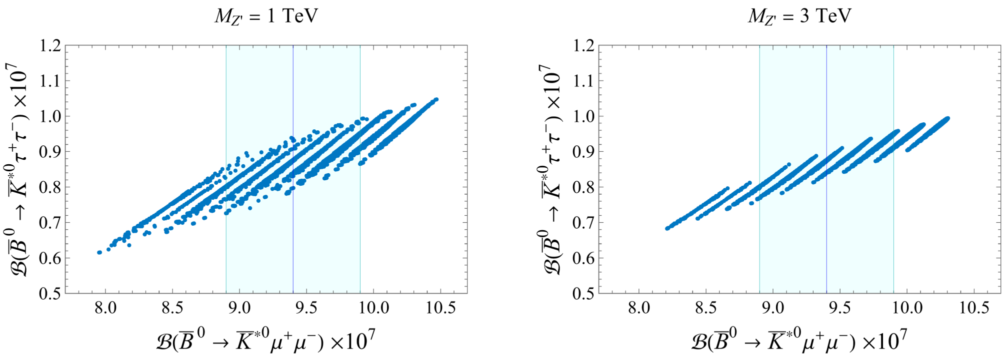

Figure 8. Correlation between $\mathcal{B}(\bar{B}^0 \to \bar{K}^{*0}\mu^+\mu^-)$ and $\mathcal{B}(\bar{B}^0 \to \bar{K}^{*0}\tau^+\tau^-)$ for $M_{Z'} = 1\,\text{TeV}$ (left panel) and $M_{Z'} = 3\,\text{TeV}$ (right panel). The shaded band corresponds to the experimental result $\mathcal{B}(\bar{B}^0 \to \bar{K}^{*0}\mu^+\mu^-) = (9.4 \pm 0.5) \times 10^{-7}$ [30].

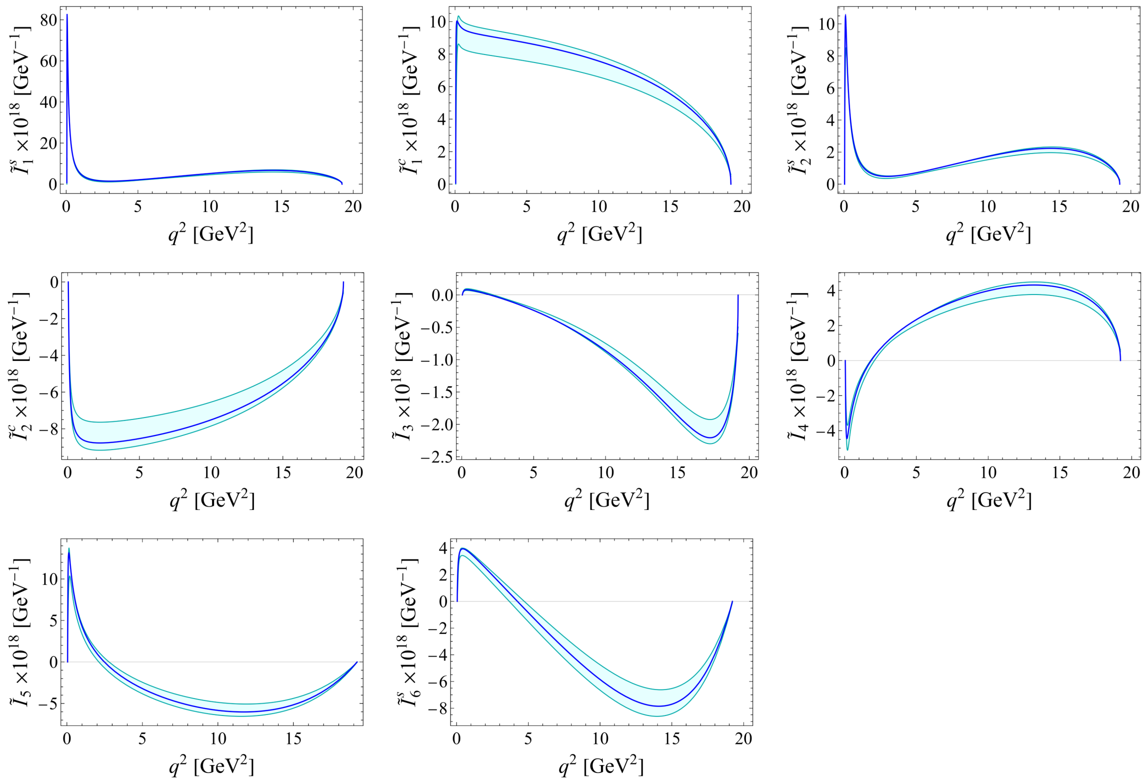

Figure 9. Angular coefficient functions $\tilde{I}_i^{(a)}(q^2)$ for $\bar{B}^0 \to \bar{K}^{*0}(K\pi)\mu^+\mu^-$. The continuous line is the SM result for the central value of the form factor parameters, the light shaded region the result in the ABCD model varying the parameters in the allowed ranges, with $M_{Z'} = 1\,\text{TeV}$.

(for $M_{Z'} = 3\,\text{TeV}$ the results do not change sensibly). The functions $I_{6c,7,8,9}$ vanish in SM; in the ABCD model they are about 10^{-6} times smaller than all others, therefore we do not display them. In the figures, the dark continuous line is the SM result for the central values of the form factor parameters, the light shaded band the ABCD result. Modest deviations with respect to SM are possible, they are more pronounced in the case of τ.

For the forward-backward asymmetry and the fraction F_L of longitudinally polarized K^*, eqs. (3.18), (3.19), the results are displayed in figure 11 for μ and τ. No measurement

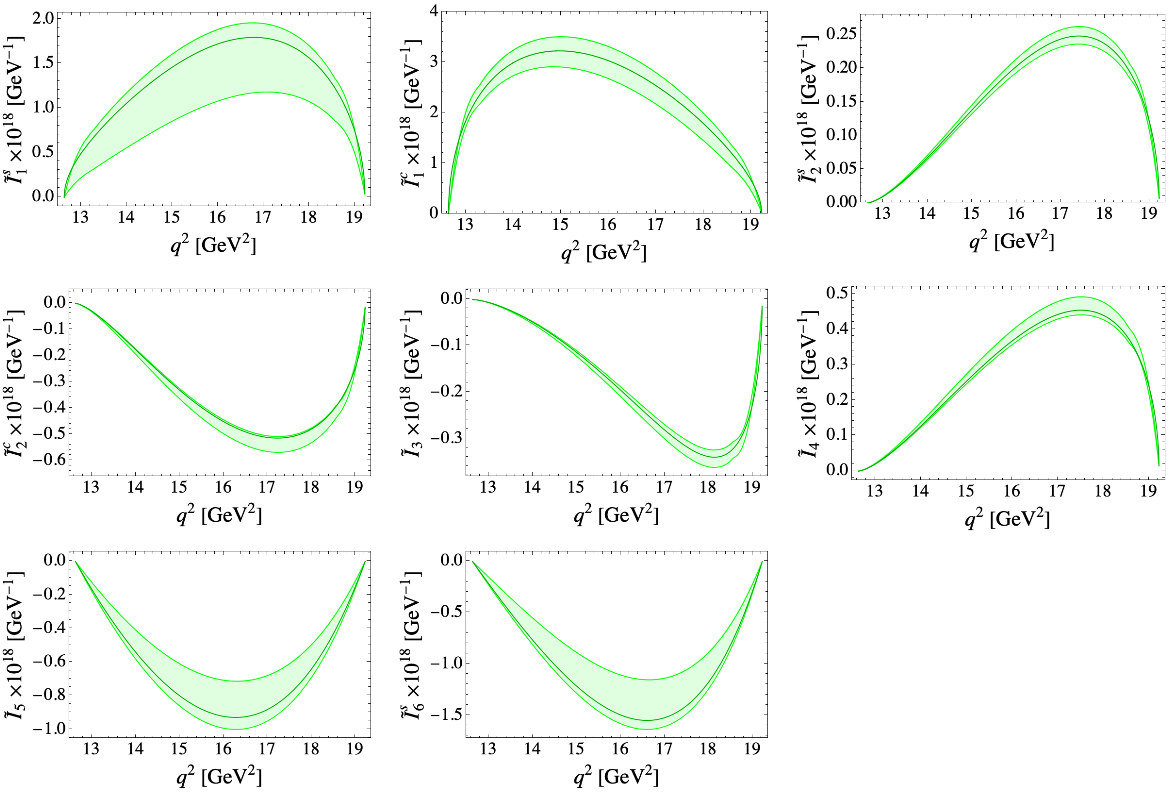

Figure 10. Angular coefficient functions for $\bar{B}^0 \to \bar{K}^{*0}(K\pi)\tau^+\tau^-$. The continuous line is the SM result for the central value of the form factor parameters, the light shaded region the result in the ABCD model varying the parameters in the allowed ranges, with $M_{Z'} = 1\,\text{TeV}$.

is available for τ. The largest deviation from SM is found in F_L at high q^2 in the τ mode. For the P-observables in (3.20) where tensions emerged [50, 85–90], we display the most significant results in figure 12. The effects obtained in the ABCD model are more pronounced for τ, namely for low q^2 the observable P_5' can differ from SM.

For $B_s \to \phi\mu^-\mu^+$, using the form factors in [76] with parameters in table 3, we find in SM: $\bar{\mathcal{B}}(B_s \to \phi\mu^-\mu^+) = (11.8 \pm 2.3) \times 10^{-7}\,(|\lambda_{ts}^*|/0.04)^2$, confirming that a higher value is foreseen for this rate with respect to the measured $\bar{\mathcal{B}}(B_s \to \phi\mu^-\mu^+)_{\text{exp}} = (8.4 \pm 0.4) \times 10^{-7}$ [30]. Measurements are not available for the τ mode: we find $\bar{\mathcal{B}}(B_s \to \phi\tau^-\tau^+) = (1.02 \pm 0.20) \times 10^{-7}\,(|\lambda_{ts}^*|/0.04)^2$ in SM. Figure 13 shows the correlation between the two LFC decays in the ABCD model: the plot for $M_{Z'} = 1\,\text{TeV}$ shows that the range for the τ mode is $\bar{\mathcal{B}}(B_s \to \phi\tau^-\tau^+) = (0.9 \pm 0.25) \times 10^{-7}$, for $M_{Z'} = 3\,\text{TeV}$ the range is $\bar{\mathcal{B}}(B_s \to \phi\tau^-\tau^+) = (0.9 \pm 0.2) \times 10^{-7}$. However, since $\bar{\mathcal{B}}(B_s \to \phi\mu^-\mu^+)_{\text{exp}}$ is not reproduced, a puzzle remains unsolved for this mode. If the measurement is confirmed, the first issue to scrutinise is the uncertainty of the $B_s \to \phi$ form factors.

4.1.2 Exclusive lepton flavour violating modes $b \to s\ell_1^-\ell_2^+$ ($\ell_1 \neq \ell_2$)

A feature of the ABCD model is that correlations are generated between lepton flavour conserving and lepton flavour violating modes. In table 1 we quote the predictions for a set of LFV modes, for $M_{Z'} = 1\,\text{TeV}$ and $3\,\text{TeV}$. The predictions can be further constrained

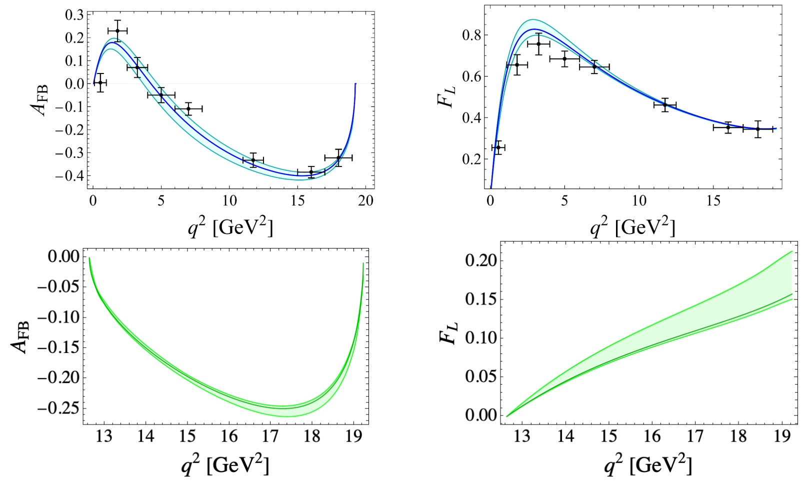

Figure 11. Forward-backward asymmetry $A_{FB}(q^2)$ (left) and K^* polarization fraction $F_L(q^2)$ (right plots) for $\bar{B}^0 \to \bar{K}^{*0}(K\pi)\mu^+\mu^-$ (top panels) and $\bar{B}^0 \to \bar{K}^{*0}(K\pi)\tau^+\tau^-$ (bottom panels). The dark continuous line is the SM result, the shaded region the ABCD result for $M_{Z'} = 1\,\text{TeV}$. The black dots in the top panels correspond to the LHCb measurement [88].

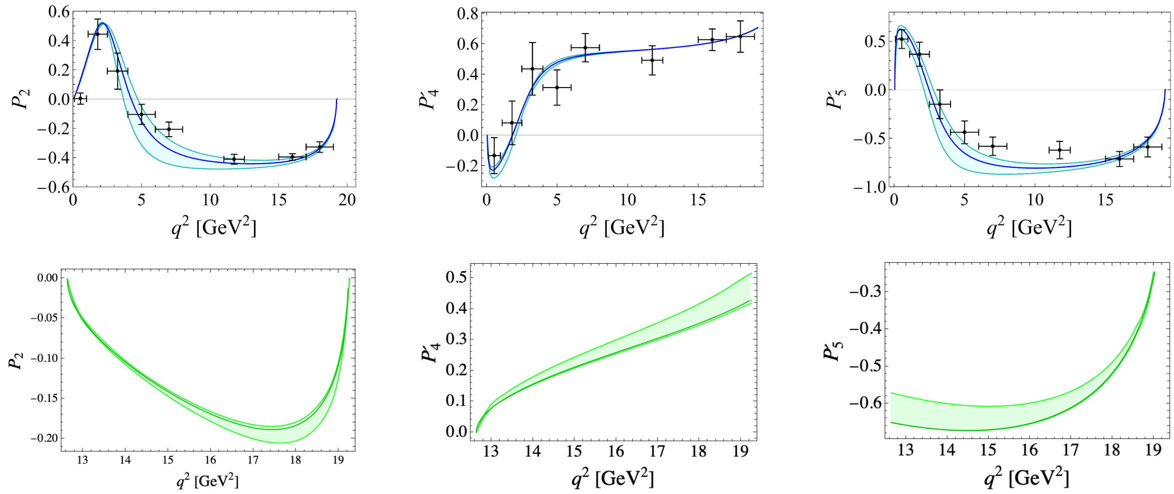

Figure 12. Angular P-observables in eq. (3.20) for $\bar{B}^0 \to \bar{K}^{*0}(K\pi)\mu^+\mu^-$ (top panels) and $\bar{B}^0 \to \bar{K}^{*0}(K\pi)\tau^+\tau^-$ (bottom panels). The black dots in the top panels correspond to LHCb measurement [88]. Same color code as in figure 11.

requiring agreement of the rates of corresponding LFC modes with experiment. In the table we quote the unconstrained result and the one constrained by the corresponding LFC process. The current experimental upper bounds for the LFV modes are also included in the table, they are expected to be sensibly improved in the near future.[8]

Figure 14 shows the correlation between the branching ratios of the LFC $B_s \to \mu^+\mu^-$ and LFV $B_s \to \tau^+\mu^-$ modes for the two values of $M_{Z'}$. The experimental upper bound for $\bar{\mathcal{B}}(B_s \to \tau^+\mu^-)$ is quoted in table 1. In the ABCD model the branching ratio of the LFV $\tau^+\mu^-$ mode can be comparable to that of the LFC $\mu^+\mu^-$ mode. Indeed, the decay to same

[8] Recent experimental investigations of $\bar{B}^0 \to \bar{K}^{*0}\tau^+\mu^-$ are described in [92, 93].

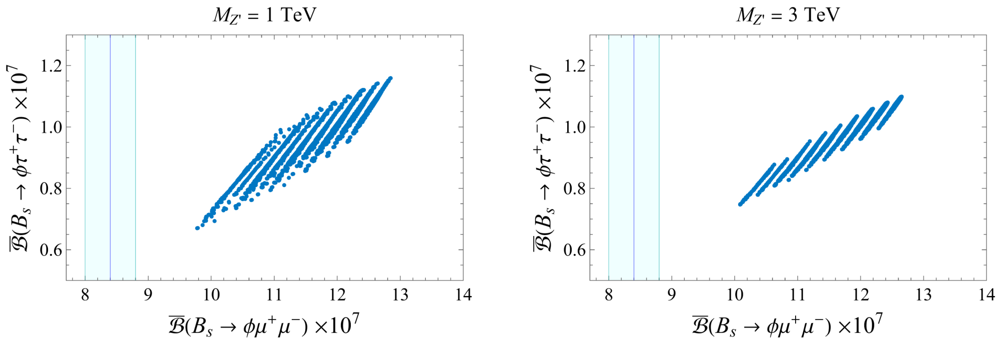

Figure 13. Correlation between $\bar{\mathcal{B}}(B_s \to \phi\mu^+\mu^-)$ and $\bar{\mathcal{B}}(B_s \to \phi\tau^+\tau^-)$ for $M_{Z'} = 1\,\text{TeV}$ (left panel) and $M_{Z'} = 3\,\text{TeV}$ (right panel). The shaded vertical band corresponds to the result $\bar{\mathcal{B}}(B_s \to \phi\mu^+\mu^-)|_{\text{exp}} = (8.4 \pm 0.4) \times 10^{-7}$ quoted in [30].

LFV mode	$\mathcal{B}^{(1)} \times 10^9$	$\mathcal{B}^{(2)} \times 10^9$	$\mathcal{B}^{(3)} \times 10^{11}$	$\mathcal{B}^{(4)} \times 10^{13}$	experiment
$B_s \to \tau^+\mu^-$	$0.00 \div 2.10$	$0.00 \div 1.60$	$0.00 \div 1.20$	$0.00 \div 9.20$	$< 4.2 \times 10^{-5}$ [30]
$\bar{B}^0 \to \bar{K}^{*0}\tau^+\mu^-$	$0.00 \div 2.90$	$0.00 \div 1.15$	$0.00 \div 1.60$	$0.00 \div 5.10$	$< 1.0 \times 10^{-5}$ [30]
$B_s \to \phi\tau^+\mu^-$	$0.00 \div 3.43$	$0.00 \div 2.60$	$0.00 \div 1.95$	$0.00 \div 6.10$	$< 1.0 \times 10^{-5}$ [91]
$B_s \to \tau^+\mu^-$	$0.00 \div 2.30$	$0.00 \div 0.14$	$0.00 \div 1.10$	$0.00 \div 1.05$	$< 4.2 \times 10^{-5}$ [30]
$\bar{B}^0 \to \bar{K}^{*0}\tau^+\mu^-$	$0.00 \div 3.10$	$0.00 \div 0.20$	$0.00 \div 1.53$	$0.00 \div 1.42$	$< 1.0 \times 10^{-5}$ [30]
$B_s \to \phi\tau^+\mu^-$	$0.00 \div 3.70$	$0.00 \div 0.25$	$0.00 \div 1.80$	$0.00 \div 1.70$	$< 1.0 \times 10^{-5}$ [91]

Table 1. Ranges of branching fractions of LFV B, B_s decays in the scenario A of the ABCD model. The first three rows correspond to $M_{Z'} = 1\,\text{TeV}$, the last three rows to $M_{Z'} = 3\,\text{TeV}$. The four quoted ranges are obtained after imposing the constraints from the upper bounds on LFV charged lepton decay modes specified in table 2: $\mathcal{B}^{(1)}$ from $\tau^- \to \mu^-\mu^+\mu^-$, $\mathcal{B}^{(2)}$ from $\mathcal{B}(\mu^- \to e^-\gamma)$, $\mathcal{B}^{(3)}$ from $\mu^- \to e^-e^+e^-$, $\mathcal{B}^{(4)}$ from $\mu^- \to e^-$ conversion in titanium. The experimental upper bounds (at 90% C.L.) are quoted in the last column.

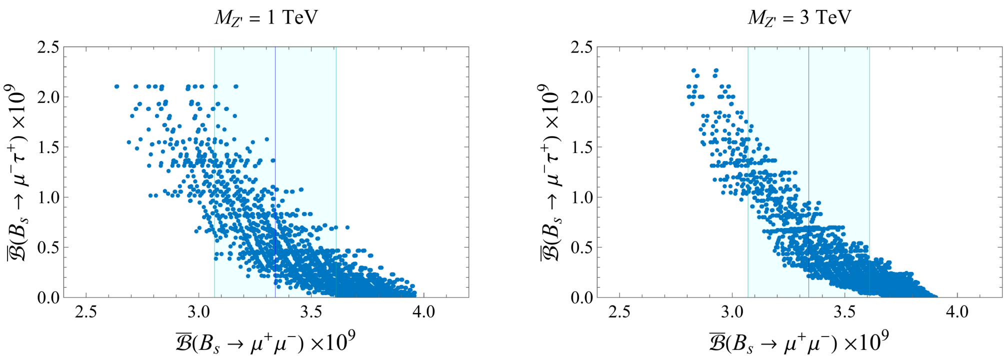

Figure 14. Correlation between the branching fractions $\bar{\mathcal{B}}(B_s \to \mu^+\mu^-)$ and $\bar{\mathcal{B}}(B_s \to \tau^+\mu^-)$ for $M_{Z'} = 1\,\text{TeV}$ (left panel) and $M_{Z'} = 3\,\text{TeV}$ (right panel). The shaded vertical band corresponds to the experimental world average [30].

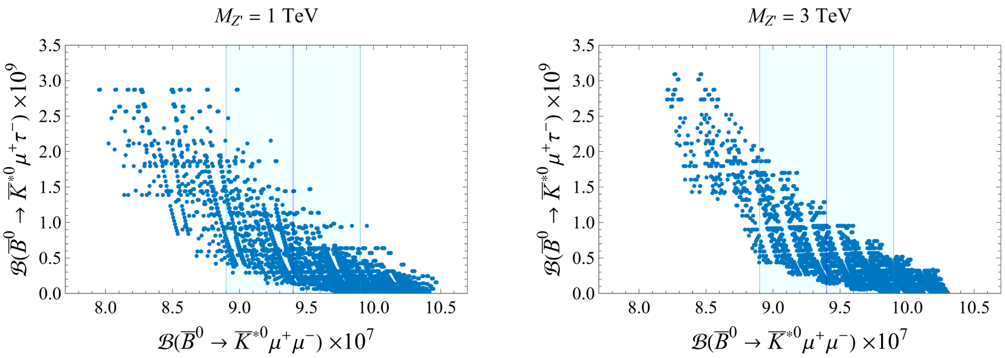

Figure 15. Correlation between $\mathcal{B}(\bar{B}^0 \to \bar{K}^{*0}\mu^+\mu^-)$ and $\mathcal{B}(\bar{B}^0 \to \bar{K}^{*0}\mu^+\tau^-)$ for $M_{Z'} = 1\,\mathrm{TeV}$ (left panel) and $M_{Z'} = 3\,\mathrm{TeV}$ (right panel). Same color code as in figure 8.

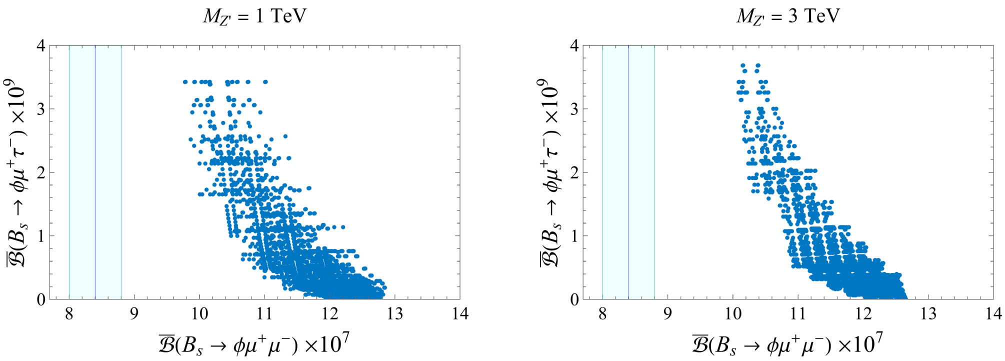

Figure 16. Correlation between $\bar{\mathcal{B}}(B_s \to \phi\mu^+\mu^-)$ and $\bar{\mathcal{B}}(B_s \to \phi\mu^+\tau^-)$ for $M_{Z'} = 1\,\mathrm{TeV}$ (left panel) and $M_{Z'} = 3\,\mathrm{TeV}$ (right panel). Same color code as in figure 13.

flavour leptons is determined only by the C_{10} term, while for $\ell_1 \neq \ell_2$ also C_9 contributes. Moreover, the helicity suppression in the $\ell_1 = \ell_2 = \mu$ mode is lifted in the $\tau^+\mu^-$ mode producing a sizable enhancement.

While for the LFC modes the results do not sensibly change varying $M_{Z'}$ from 1 TeV to 3 TeV, this is not true for the LFV modes, since ABCD does not predict large deviations from SM: increasing the Z' mass, the SM results are approached. For modes allowed in SM, the deviations are small even for small values of $M_{Z'}$. On the other hand, for modes forbidden in SM, increasing $M_{Z'}$ results in a sensible decrease of the branching fractions. The same observation holds for $\bar{B}^0 \to \bar{K}^{*0}\tau^+\mu^-$: the branching fraction predicted in the ABCD model is quoted in table 1 both without and with the constraint given by the measured $\mathcal{B}(\bar{B}^0 \to \bar{K}^{*0}\mu^+\mu^-)$. As we discuss below, constraints provided by LFV leptonic decays further reduce the range for this rate. Predictions for $B_s \to \phi\tau^+\mu^-$ are presented in table 1 and in figure 16.

4.2 Correlations among lepton flavour violating processes in the quark and lepton sectors

Since the Z' couplings to leptons and quarks involve the same pair of parameters, ϵ_1 and ϵ_2, correlations can be established among observables in the different sectors. Particularly

JHEP12(2025)069

LFV mode	$\mathcal{B}$ experiment
$\tau^- \to \mu^-\mu^+\mu^-$	$< 2.1 \times 10^{-8}$ [30]
$\mu^- \to e^-\gamma$	$< 1.5 \times 10^{-13}$ [94]
$\mu^- \to e^-e^+e^-$	$< 1.0 \times 10^{-12}$ [30, 95]
$\mu^- \to e^-$ conversion in ${}^{48}_{22}\mathrm{Ti}$	$< 4.3 \times 10^{-12}$ [65, 96]

Table 2. Experimental upper bounds (at 90 % C.L.) for LFV charged lepton modes. The branching fraction for the $\mu^- \to e^-$ conversion is defined in eq. (3.33).

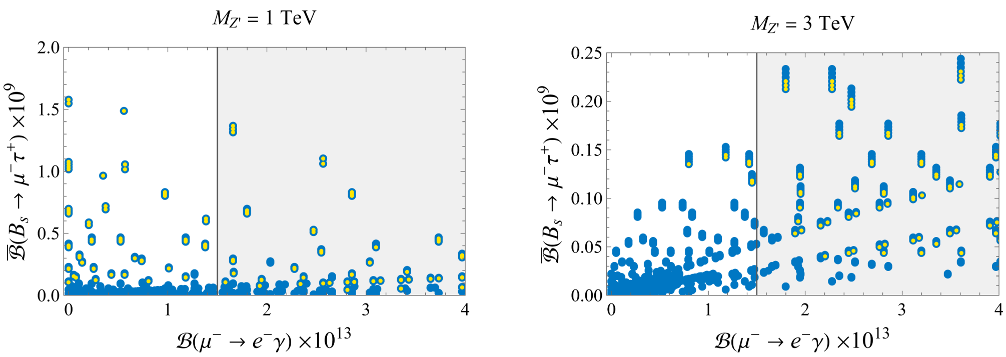

Figure 17. Correlation between $\bar{\mathcal{B}}(B_s \to \tau^+\mu^-)$ and $\mathcal{B}(\mu^- \to e^-\gamma)$ for $M_{Z'} = 1\,\mathrm{TeV}$ (left panel) and $M_{Z'} = 3\,\mathrm{TeV}$ (right panel). The vertical line indicates the experimental upper bound $\mathcal{B}(\mu^- \to e^-\gamma) < 1.5 \times 10^{-13}$ (at 90% CL) [94]. The light yellow points are selected requiring that the LFC $\bar{\mathcal{B}}(B_s \to \mu^+\mu^-)$ agrees within 1σ with experiment.

relevant are the correlations between the LFV $b \to s\ell_1^+\ell_2^-$ modes and the LFV leptonic decays $\mu^- \to e^-\gamma$, $\tau^- \to \mu^-\mu^+\mu^-$, $\mu^- \to e^-e^+e^-$, and the $\mu^- \to e^-$ conversion in nuclei. As we shall see, in the scenario A of the ABCD model the upper bounds on the last four channels play a hierarchical role in constraining the branching ratios of LFV B and B_s decays. Their combined effect prevents the branching fractions of LFV B and B_s decays from exceeding $\mathcal{O}(10^{-12})$.

It is useful to analyse the individual constraints from the four leptonic processes, which in scenarios different from scenario A depend on distinct parameters. This provides us with a guidance on possible modifications of the scenario. For instance, since $\tau^- \to \mu^-\mu^+\mu^-$ provides the weakest constraint, one may consider assigning a different role to the third lepton family compared to the other two: we defer such an investigation to future work. In the following we analyze the impact of $\tau^- \to \mu^-\mu^+\mu^-$ and $\mu^- \to e^-\gamma$, then we consider the most stringent channels $\mu^- \to e^-e^+e^-$ and $\mu^- \to e^-$ conversion in nuclei.

4.2.1 Rare $B_{(s)}$ decays versus $\tau^- \to \mu^-\mu^+\mu^-$ and $\mu^- \to e^-\gamma$

The correlations involving $\tau^- \to \mu^-\mu^+\mu^-$, with the experimental upper bound $\mathcal{B}(\tau^- \to \mu^-\mu^+\mu^-) < 2.1 \times 10^{-8}$ [30] do not provide significant constraints for B_s and B modes. Accounting for the measurement of the width of $B_s \to \mu^+\mu^-$, the largest value for $\mathcal{B}(\tau^- \to \mu^-\mu^+\mu^-)$ is about 1.2×10^{-8}.

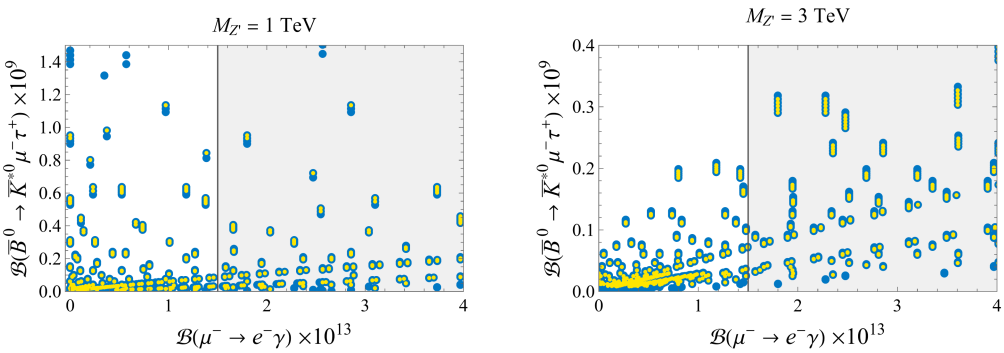

Figure 18. Correlation between $\mathcal{B}(\bar{B}^0 \to \bar{K}^{*0}\tau^+\mu^-)$ and $\mathcal{B}(\mu^- \to e^-\gamma)$ for $M_{Z'} = 1\,\text{TeV}$ (left panel) and $M_{Z'} = 3\,\text{TeV}$ (right panel). The vertical line corresponds to the experimental upper bound for $\mathcal{B}(\mu^- \to e^-\gamma)$ [94]. The light yellow points are selected requiring that the LFC $\mathcal{B}(\bar{B}^0 \to \bar{K}^{*0}\mu^+\mu^-)$ agrees within 1σ with experiment.

$\mu^- \to e^-\gamma$ puts more stringent limits. Figure 17 shows the correlation between $\bar{\mathcal{B}}(B_s \to \tau^+\mu^-)$ and $\mathcal{B}(\mu^- \to e^-\gamma)$ for $M_{Z'} = 1\,\text{TeV}$ and $3\,\text{TeV}$. The dark points show the results without imposing constraints from LFC mode, the light points the results obtained imposing that the measured $\bar{\mathcal{B}}(B_s \to \mu^+\mu^-)$ is recovered. The upper bound is displayed $\mathcal{B}(\mu^- \to e^-\gamma) < 1.5 \times 10^{-13}$ (at 90% CL) recently established by the MEG II Collaboration [94] which has improved the previous limit $\mathcal{B}(\mu^- \to e^-\gamma) < 4.2 \times 10^{-13}$ (at 90% CL) [97]. The bound reduces the room for $\bar{\mathcal{B}}(B_s \to \tau^+\mu^-)$. This provides us with a clear example of the most peculiar feature of the ABCD model, the interplay between quark and lepton observables. Within the model, quite large values of $\mathcal{B}(\mu^- \to e^-\gamma)$ could be obtained, however, the requirement that the rate of $B_s \to \mu^+\mu^-$ agrees with experiment suppresses $\mathcal{B}(\mu^- \to e^-\gamma)$. The correlation between $\mathcal{B}(\bar{B}^0 \to \bar{K}^{*0}\tau^+\mu^-)$ and $\mathcal{B}(\mu^- \to e^-\gamma)$ is displayed in figure 18, and similar remarks hold: the bound on $\mathcal{B}(\mu^- \to e^-\gamma)$ [94] reduces the allowed range for $\mathcal{B}(B \to K^*\tau^+\mu^-)$, see table 1. The same occurs for $B_s \to \phi\tau^+\mu^-$.

4.2.2 Rare $B_{(s)}$ decays versus $\mu^- \to e^-e^+e^-$ and $\mu^- \to e^-$ conversion in nuclei

The processes $\mu^- \to e^-e^+e^-$ and $\mu^- \to e^-$ conversion in nuclei play the major role in constraining LFV rare $B_{(s)}$ decays. Figure 19 shows that the upper limit $\mathcal{B}(\mu^- \to e^-e^+e^-) < 1 \times 10^{-12}$ (at 90% CL) [30, 95] significantly reduces $\bar{\mathcal{B}}(B_s \to \tau^+\mu^-)$ and $\mathcal{B}(\bar{B}^0 \to \bar{K}^{*0}\tau^+\mu^-)$ both for $M_{Z'} = 1\,\text{TeV}$ and for $M_{Z'} = 3\,\text{TeV}$. After imposing this bound their largest allowed values are $\mathcal{O}(10^{-11})$, see table 2. Muon conversion in nuclei provides the most stringent constraint, as displayed in figure 20. The largest allowed value for $\bar{\mathcal{B}}(B_s \to \tau^+\mu^-)$ and $\mathcal{B}(\bar{B}^0 \to \bar{K}^{*0}\tau^+\mu^-)$ are reduced to $\mathcal{O}(10^{-13})$, see table 2.

A summary of the impact of the lepton decays on $\bar{\mathcal{B}}(B_s \to \tau^+\mu^-)$ and $\mathcal{B}(\bar{B}^0 \to \bar{K}^{*0}\tau^+\mu^-)$ is in figure 22, where we plot their correlation when subsequent constraints from LFV charged lepton decay modes are imposed. It is instructive to examine the mutual impact of different LFV lepton decays. As an example, figure 21 shows the constraints imposed by the experimental upper bound for $\mathcal{B}(\mu^- \to e^-e^+e^-)$ on $\mathcal{B}(\mu^- \to e^-)$ and $\mathcal{B}(\tau^- \to \mu^-\mu^+\mu^-)$: in both cases the allowed ranges are substantially reduced.

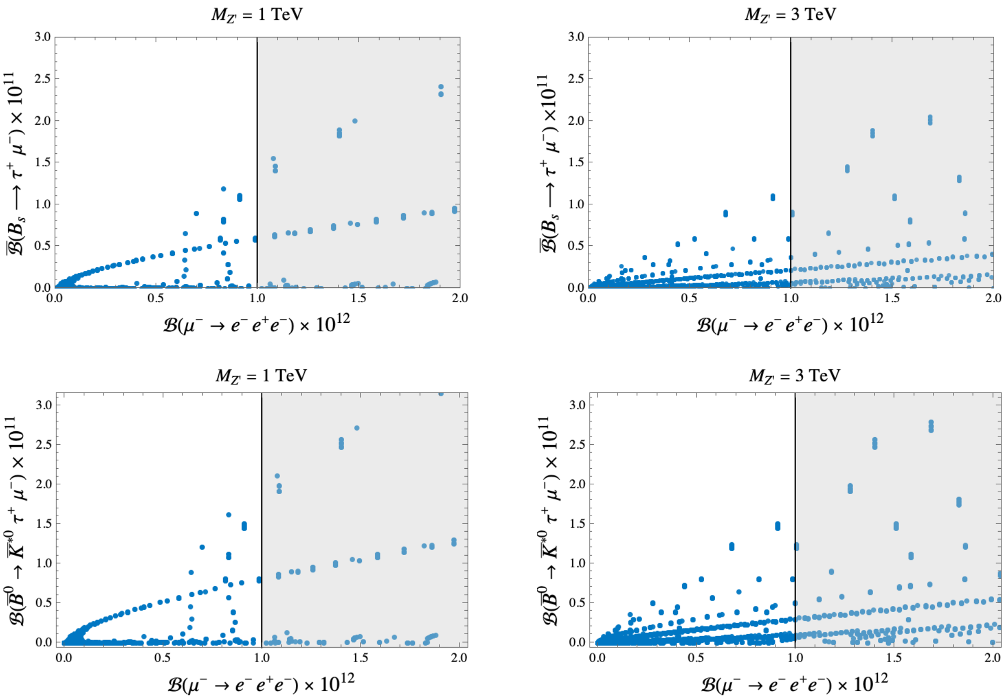

Figure 19. Correlation between $\bar{\mathcal{B}}(B_s \to \tau^+\mu^-)$ and $\mathcal{B}(\mu^- \to e^-e^+e^-)$ (top panels) and between $\mathcal{B}(\bar{B}^0 \to \bar{K}^{*0}\tau^+\mu^-)$ and $\mathcal{B}(\mu^- \to e^-e^+e^-)$ (bottom panels), for $M_{Z'} = 1\,\text{TeV}$ (left panel) and $M_{Z'} = 3\,\text{TeV}$ (right panel). The gray band corresponds to the upper bound $\mathcal{B}(\mu^- \to e^-e^+e^-) < 1 \times 10^{-12}$ (at 90% CL) [30, 95].

The scrutiny of $\mu^- \to e^-e^+e^-$ and $\mu^- \to e^-$ conversion will be the focus of future experimental programs, in particular at the COMET [98], Mu2e [99] and Mu3e [100] facilities that aim at an unprecedented sensitivity. The experimental bounds used in our study are based on measurements performed more than two decades ago, and have been obtained relying on theoretical formulae and approximations that need to be reconsidered. For example, for $\mu^- \to e^-e^+e^-$ the quoted upper bound has been obtained assuming a constant decay amplitude over the entire phase space. Such assumptions will be refined in the future studies.

4.2.3 Rare $B_{(s)}$ decays versus Δa_μ

As for the Z' contribution to the muon anomalous magnetic moment, Δa_μ vs $\mathcal{B}(\bar{B}^0 \to \bar{K}^{*0}\tau^+\mu^-)$ is shown in figure 23. Δa_μ turns out to be negative, it reaches at most $\Delta a_\mu \sim -10^{-12}$, a size similar to subleading hadron contributions such as the hadronic light-by-light contribution [13].

5 Conclusions

The search for BSM is facing the evidence that tensions with the SM predictions are spotted, but they are small. For example, the flavour anomalies are below the level of significance to claim the evidence of new physics. Being confident on NP, we have attempted to justify the absence of large deviations: we have scrutinised channels where anomalies have been detected together with processes strictly forbidden in SM, the charged lepton flavour violating modes,

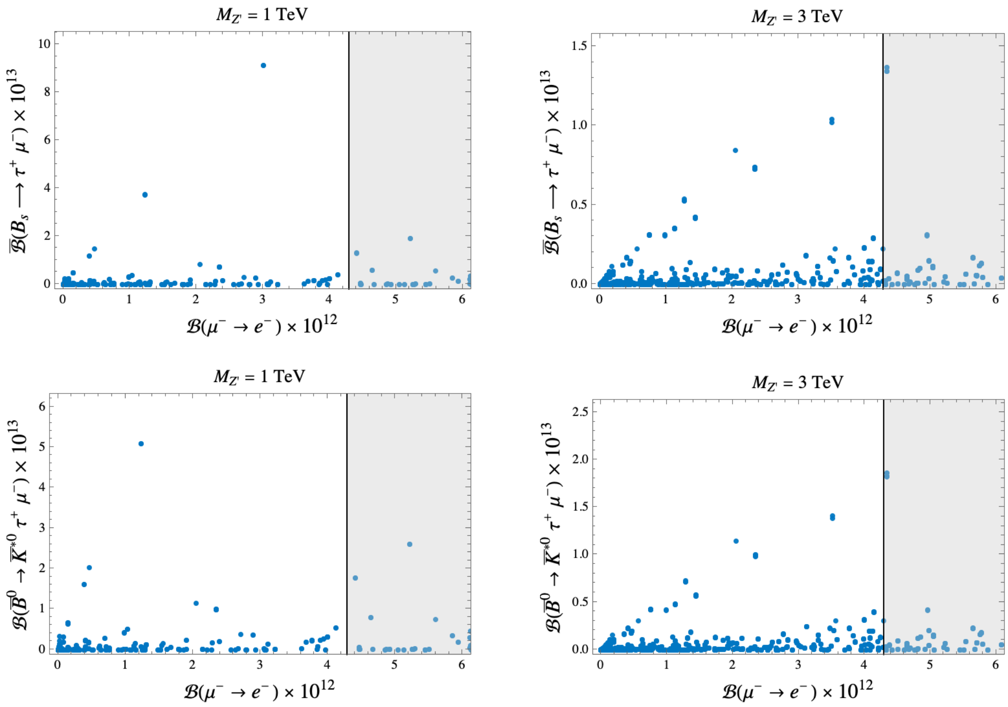

Figure 20. Correlation between $\bar{\mathcal{B}}(B_s \to \tau^+\mu^-)$ and $\mathcal{B}(\mu^- \to e^-)$ due to conversion in nuclei (top panels) and between $\mathcal{B}(\bar{B}^0 \to \bar{K}^{*0}\tau^+\mu^-)$ and $\mathcal{B}(\mu^- \to e^-)$ due to conversion in nuclei (bottom panels), for $M_{Z'} = 1\,\text{TeV}$ (left panel) and $M_{Z'} = 3\,\text{TeV}$ (right panel). The gray band corresponds to the upper bound $\mathcal{B}(\mu^- \to e^-) < 4.3 \times 10^{-12}$ (at 90% CL) [65].

and the correlations among them. In a simple extension of the SM, the ABCD model, the new gauge boson Z' has flavour conserving and flavour violating generation-dependent couplings to fermions. The model is based on a special solution of the gauge anomaly cancellation equations which relates the quark and lepton couplings to Z'. The flavour observables in the two sectors are intertwined, producing nontrivial correlations.

As noticed when the model has been formulated [1], quark and lepton sectors mutually act to prevent large deviations from SM, a welcome feature considering the small discrepancies with respect to SM emerged by measurements of flavour observables. Moreover, the possibility of having lepton flavour violation implies that modes such as those induced by $b \to s\ell_1^-\ell_2^+$ with $\ell_1 \neq \ell_2$, can occur and are correlated both to purely leptonic LFV processes, $\mu^- \to e^-\gamma$, $\tau^- \to \mu^-\mu^+\mu^-$, $\mu^- \to e^-e^+e^-$ and $\mu^- \to e^-$ conversion in nuclei, as well as to the LFC $b \to s\ell^-\ell^+$ transitions.

To summarize our main findings, we remark that:

- Imposing $\Delta F = 2$ constraints, the NP contributions to the Wilson coefficients $\mathrm{Re}(C_9^{\mathrm{NP}})_{\ell\ell}$ and $\mathrm{Re}(C_{10}^{\mathrm{NP}})_{\ell\ell}$, $\ell = \mu, \tau$, are found to be at the $\simeq 10\%$ level of the corresponding SM coefficients. The analogous LFV coefficients $\mathrm{Re}(C_9^{\mathrm{NP}})_{\mu\tau}$ and $\mathrm{Re}(C_{10}^{\mathrm{NP}})_{\mu\tau}$ are of the comparable size to $\mathrm{Re}(C_{9(10)}^{\mathrm{NP}})_{\mu\mu}$, see figures 4–6.

- The LFV $B_{(s)}$ decays are constrained by LFC modes and by purely leptonic LFV processes in a hierarchical way; the weakest bounds arise from the LFC decays, see

JHEP12(2025)069

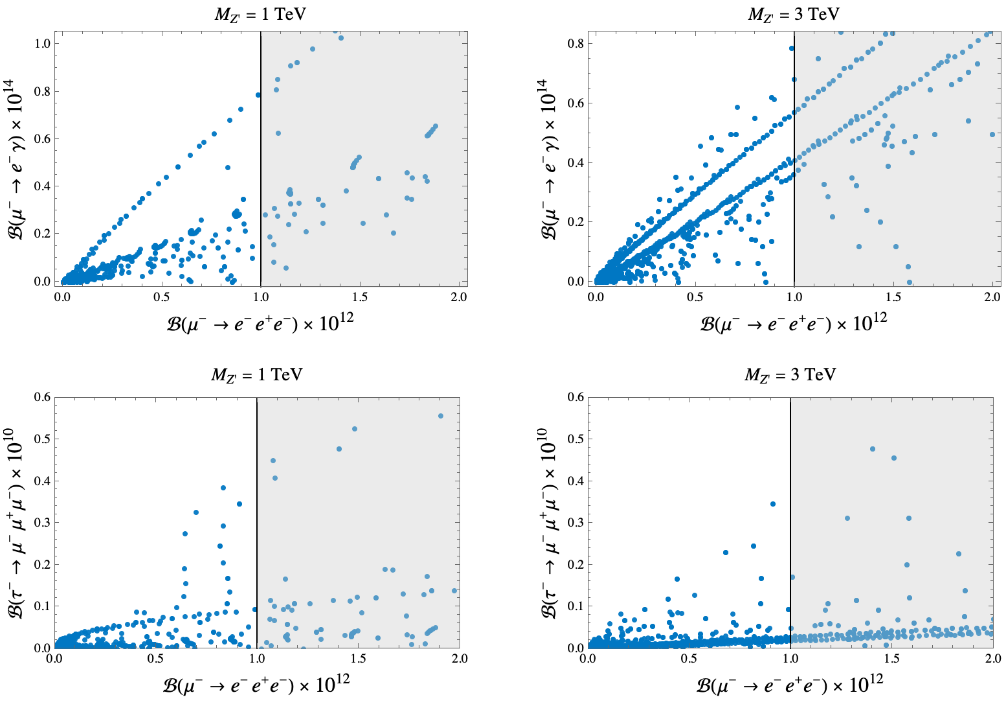

Figure 21. Correlation between $\mathcal{B}(\mu^- \to e^- e^+ e^-)$ and $\mathcal{B}(\mu^- \to e^-\gamma)$ (top panels) and between $\mathcal{B}(\mu^- \to e^- e^+ e^-)$ and $\mathcal{B}(\tau^- \to \mu^- \mu^+ \mu^-)$ (bottom panels), for $M_{Z'} = 1\,\text{TeV}$ (left panel) and $M_{Z'} = 3\,\text{TeV}$ (right panel). The gray band corresponds to the upper bound $\mathcal{B}(\mu^- \to e^- e^+ e^-) < 1 \times 10^{-12}$ (at 90% CL) [30, 95].

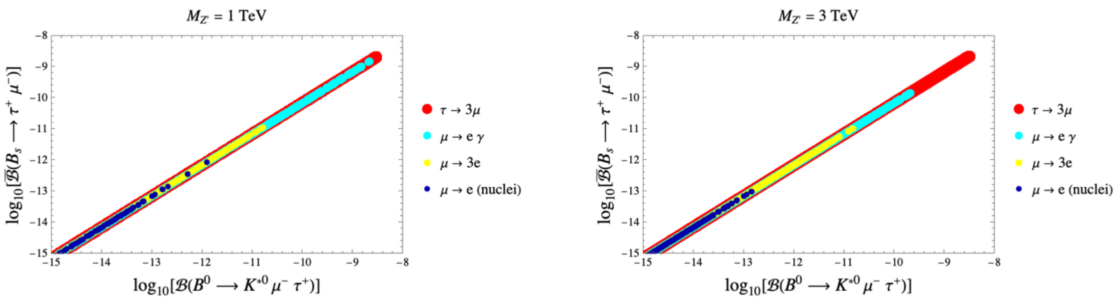

Figure 22. Correlation between $\bar{\mathcal{B}}(B_s \to \tau^+\mu^-)$ and $\mathcal{B}(\bar{B}^0 \to \bar{K}^{*0}\tau^+\mu^-)$ when constraints from LFV charged lepton decay modes are subsequently imposed as specified in the legenda, for $M_{Z'} = 1\,\text{TeV}$ (left panel) and $M_{Z'} = 3\,\text{TeV}$ (right panel).

figures 14–16, then by $\tau^- \to \mu^-\mu^+\mu^-$, $\mu^- \to e^-\gamma$ and by $\mu^- \to e^-e^+e^-$ and $\mu^- \to e^-$ conversion in nuclei, figures 17–18.

- The role of quark and lepton observables to mutually constrain each other is visible in the results in table 1 and in figure 22.

The above results are relevant for the NP searches at the new facilities planned within the future strategy for particle physics.

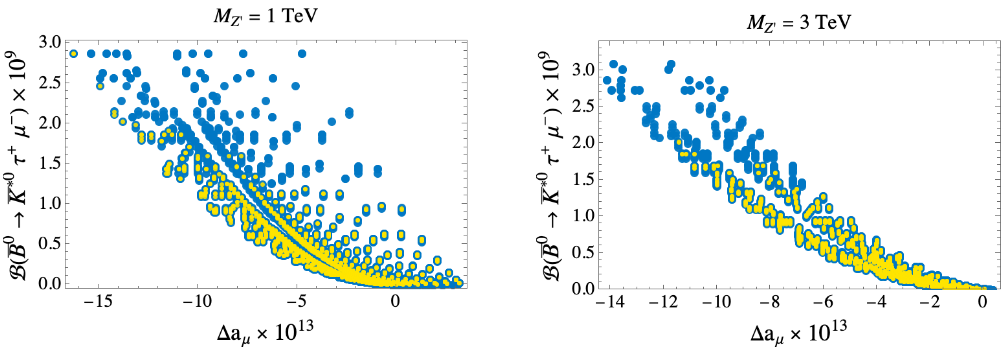

Figure 23. Correlation between $\mathcal{B}(\bar{B}^0 \to \bar{K}^{*0}\tau^+\mu^-)$ and Δa_μ for $M_{Z'} = 1\,\text{TeV}$ (left panel) and $M_{Z'} = 3\,\text{TeV}$ (right panel). The light yellow points are selected requiring that the LFC $\mathcal{B}(\bar{B}^0 \to \bar{K}^{*0}\mu^+\mu^-)$ agrees with experiment at 1σ.

Acknowledgments

F.D.F. thanks the coauthors of [1]. We thank A.J. Buras for very useful discussions. This study has been carried out within the INFN project (Iniziativa Specifica) SPIF. The research has been partly funded by the European Union — Next Generation EU through the research Grant No. P2022Z4P4B "SOPHYA — Sustainable Optimised PHYsics Algorithms: fundamental physics to build an advanced society" under the program PRIN 2022 PNRR of the Italian Ministero dell'Università e Ricerca (MUR).

A $\quad B_q \to V$ local form factors

We use the standard parametrization of the $B_q \to V$ ($q = d, s$, $V = K^*, \phi$) matrix elements of local currents in terms of form factors:

$$\begin{aligned}\langle V(p',\epsilon)|\bar{s}\gamma_\mu(1-\gamma_5)b|B_q(p)\rangle = {} & \epsilon_{\mu\nu\alpha\beta}\epsilon^{*\nu}p^\alpha p'^\beta \frac{2V(q^2)}{m_{B_q}+m_V} \\ & - i\left[\epsilon^*_\mu(m_{B_q}+m_V)A_1(q^2) - (\epsilon^*\cdot q)(p+p')_\mu \frac{A_2(q^2)}{m_{B_q}+m_V}\right. \\ & \left. - (\epsilon^*\cdot q)\frac{2m_V}{q^2}(A_3(q^2)-A_0(q^2))q_\mu\right], \end{aligned} \tag{A.1}$$

$$\begin{aligned}\langle V(p',\epsilon)|\bar{s}\sigma_{\mu\nu}q^\nu(1+\gamma_5)b|B_q(p)\rangle = {} & i\epsilon_{\mu\nu\alpha\beta}\epsilon^{*\nu}p^\alpha p'^\beta\, 2\,T_1(q^2) \\ & + \left[\epsilon^*_\mu(m^2_{B_q}-m^2_V) - (\epsilon^*\cdot q)(p+p')_\mu\right] T_2(q^2) \\ & + (\epsilon^*\cdot q)\left[q_\mu - \frac{q^2}{m^2_{B_q}-m^2_V}(p+p')_\mu\right] T_3(q^2)\,, \end{aligned} \tag{A.2}$$

with $q = p - p'$ and ϵ the V polarization vector. The form factors are not all independent: A_3 is given by

$$A_3(q^2) = \frac{m_{B_q}+m_V}{2m_V}A_1(q^2) - \frac{m_{B_q}-m_V}{2m_V}A_2(q^2) \tag{A.3}$$

JHEP12(2025)069

$B \to K^*$	m_R (GeV)	α_0	α_1	α_2
V	5.415	0.34 ± 0.04	-1.05 ± 0.24	2.37 ± 1.39
A_1	5.829	0.27 ± 0.03	0.30 ± 0.19	-0.11 ± 0.48
A_0	5.366	0.36 ± 0.05	-1.04 ± 0.27	1.12 ± 1.35
A_{12}	5.829	0.26 ± 0.03	0.60 ± 0.20	0.12 ± 0.84
T_1	5.415	0.28 ± 0.03	-0.89 ± 0.19	1.95 ± 1.10
T_2	5.829	0.28 ± 0.03	0.40 ± 0.18	0.36 ± 0.51
T_{23}	5.829	0.67 ± 0.08	1.48 ± 0.49	1.92 ± 1.96
$B_s \to \phi$	m_R (GeV)	α_0	α_1	α_2
V	5.415	0.39 ± 0.03	-1.03 ± 0.25	3.50 ± 1.55
A_1	5.829	0.30 ± 0.03	0.48 ± 0.19	0.29 ± 0.65
A_0	5.366	0.39 ± 0.05	-0.78 ± 0.26	2.41 ± 1.48
A_{12}	5.829	0.25 ± 0.03	0.76 ± 0.20	0.71 ± 0.96
T_1	5.415	0.31 ± 0.03	-0.87 ± 0.19	2.75 ± 1.19
T_2	5.829	0.31 ± 0.03	0.58 ± 0.19	0.89 ± 0.71
T_{23}	5.829	0.68 ± 0.07	2.11 ± 0.46	4.94 ± 2.25

Table 3. Parameters of the $B_{(s)} \to V$ form factors in eq. (A.5) determined in [76].

with $A_3(0) = A_0(0)$. $T_1(0) = T_2(0)$ follows from the identity $\sigma_{\mu\nu}\gamma_5 = -\frac{i}{2}\epsilon_{\mu\nu\alpha\beta}\sigma^{\alpha\beta}$ (with $\epsilon_{0123} = +1$).

In our analysis we use the determination in [76] based on light-cone QCD sum rules (see also [101]). Defining the "conformal" variable

$$z(t) = \frac{\sqrt{t_+ - t} - \sqrt{t_+ - t_0}}{\sqrt{t_+ - t} + \sqrt{t_+ - t_0}} \tag{A.4}$$

with $t_\pm = (m_{B_q} \pm m_V)^2$ and $t_0 = t_+\left(1 - \sqrt{1 - \frac{t_-}{t_+}}\right)$, a generic form factor F_i is written as the sum of the first three terms of the z-expansion

$$F_i(q^2) = \frac{1}{1 - \frac{q^2}{m_{R,i}^2}} \sum_{k=0}^{2} \alpha_k^i \left[z(q^2) - z(0)\right]^k , \tag{A.5}$$

with parameters α_k^i and $m_{R,i}$. The value of $m_{R,i}$ is close to the mass of the lightest t-channel resonance involved in the various terms in (A.1), (A.2). The parameters are determined for V, A_1, A_0, A_{12} and T_1, T_2, T_{23} in [76], defining

$$\begin{aligned}
A_{12}(q^2) &= \frac{(m_{B_q} + m_V)^2 (m_{B_q}^2 - m_V^2 - q^2) A_1(q^2) - \lambda(m_{B_q}^2, m_V^2, q^2) A_2(q^2)}{16 m_{B_q} m_V^2 (m_{B_q} + m_V)} \\
T_{23}(q^2) &= \frac{(m_{B_q}^2 - m_V^2)(m_{B_q}^2 + 3m_V^2 - q^2) T_2(q^2) - \lambda(m_{B_q}^2, m_V^2, q^2) T_3(q^2)}{8 m_{B_q} m_V^2 (m_{B_q} - m_V)} .
\end{aligned} \tag{A.6}$$

To make easier to reproduce our results, we quote the values of the parameters in table 3, while their correlation matrix is in [76].

B Angular coefficient functions for $B \to K^*(K\pi)\ell_1^-\ell_2^+$

The coefficient functions $I_i^{(a)}$, for $i = 1, \dots 9$ and $a = s$, c in (3.14), can be written in terms of the transversity amplitudes

$$
\begin{aligned}
A_{\perp L,R}(q^2) &= N(q^2)\sqrt{2}\lambda_H^{1/2}\Bigg[\Big[(C_9^{\rm eff} + C_9^{\rm eff\prime}) \mp (C_{10}^{\rm eff} + C_{10}^{\rm eff\prime})\Big]\frac{V(q^2)}{m_B + m_{K^*}} \\
&\quad + \frac{2(m_b + m_s)}{q^2}(C_7^{\rm eff} + C_7^{\rm eff\prime})T_1(q^2)\Bigg], \\
A_{\parallel L,R}(q^2) &= -N(q^2)\sqrt{2}(m_B^2 - m_{K^*}^2)\Bigg[\Big[(C_9^{\rm eff} - C_9^{\rm eff\prime}) \mp (C_{10}^{\rm eff} - C_{10}^{\rm eff\prime})\Big]\frac{A_1(q^2)}{m_B - m_{K^*}} \\
&\quad + \frac{2(m_b - m_s)}{q^2}(C_7^{\rm eff} - C_7^{\rm eff\prime})T_2(q^2)\Bigg], \\
A_{0L,R}(q^2) &= -\frac{N(q^2)}{2m_{K^*}\sqrt{q^2}}\Bigg\{\Big[(C_9^{\rm eff} - C_9^{\rm eff\prime}) \mp (C_{10}^{\rm eff} - C_{10}^{\rm eff\prime})\Big] \\
&\quad \times\Big[(m_B^2 - m_{K^*}^2 - q^2)(m_B + m_{K^*})A_1(q^2) - \lambda_H\frac{A_2(q^2)}{m_B + m_{K^*}}\Big] \\
&\quad + 2(m_b - m_s)(C_7^{\rm eff} - C_7^{\rm eff\prime})\Big[(m_B^2 + 3m_{K^*}^2 - q^2)T_2(q^2) - \frac{\lambda_H}{m_B^2 - m_{K^*}^2}T_3(q^2)\Big]\Bigg\}, \\
A_{t\,L,R}(q^2) &= -\frac{N(q^2)}{\sqrt{q^2}}\lambda_H^{1/2}\big[(C_9^{\rm eff} - C_9^{\rm eff\prime}) \mp (C_{10}^{\rm eff} - C_{10}^{\rm eff\prime})\big]A_0(q^2).
\end{aligned}
\tag{B.1}
$$

The factor $N(q^2)$ reads

$$
N(q^2) = \lambda_{ts}^*\left[\frac{G_F^2\alpha^2}{3\times 2^{10}\pi^5 m_B^3}\lambda_H^{1/2}\lambda_L^{1/2}\right]^{1/2}, \tag{B.2}
$$

with $\lambda_H = \lambda(q^2, m_B^2, m_{K^*}^2)$ and $\lambda_L = \lambda(q^2, m_1^2, m_2^2)$. The expressions of the coefficient functions are:

$$
\begin{aligned}
I_1^s &= \frac{\lambda_L + 2[q^4 - (m_1^2 - m_2^2)^2]}{4q^4}\Big[|A_{\perp L}|^2 + |A_{\parallel L}|^2 + (L \to R)\Big] + \frac{4m_1m_2}{q^2}{\rm Re}\Big[A_{\perp L}A_{\perp R}^* + A_{\parallel L}A_{\parallel R}^*\Big], \\
I_1^c &= \frac{q^4 - (m_1^2 - m_2^2)^2}{q^4}\big[|A_{0L}|^2 + |A_{0R}|^2\big] + \frac{8m_1m_2}{q^2}{\rm Re}\big[A_{0L}A_{0R}^* - A_{tL}A_{tR}^*\big] \\
&\quad - 2\frac{(m_1^2 - m_2^2)^2 - q^2(m_1^2 + m_2^2)}{q^4}\Big[|A_{tL}|^2 + |A_{tR}|^2\Big], \\
I_2^s &= \frac{\lambda_L}{4q^4}\Big[|A_{\perp L}|^2 + |A_{\parallel L}|^2 + (L \to R)\Big], \\
I_2^c &= -\frac{\lambda_L}{q^4}\Big[|A_{0L}|^2 + (L \to R)\Big], \\
I_3 &= \frac{\lambda_L}{2q^4}\Big[|A_{\perp L}|^2 - |A_{\parallel L}|^2 + (L \to R)\Big], \\
I_4 &= \frac{\lambda_L}{\sqrt{2}q^4}\Big[{\rm Re}(A_{0L}A_{\parallel L}^*) + (L \to R)\Big], \\
I_5 &= \frac{\sqrt{2}\lambda_L^{1/2}}{q^2}\Bigg[{\rm Re}[A_{0L}A_{\perp L}^* - (L \to R)] - \frac{m_1^2 - m_2^2}{q^2}{\rm Re}[A_{tL}A_{\parallel L}^* + (L \to R)]\Bigg],
\end{aligned}
$$

JHEP12(2025)069

$$I_6^s = \frac{2\lambda_L^{1/2}}{q^2}\left[\mathrm{Re}(A_{\parallel L}A_{\perp L}^*) - (L\to R)\right],$$

$$I_6^c = \frac{4\lambda_L^{1/2}}{q^2}\frac{m_1^2-m_2^2}{q^2}[\mathrm{Re}(A_{0L}A_{tL}^*)+(L\to R)],$$

$$I_7 = \frac{\sqrt{2}\lambda_L^{1/2}}{q^2}\left[\mathrm{Im}[A_{0L}A_{\parallel L}^* - (L\to R)] + \frac{m_1^2-m_2^2}{q^2}\mathrm{Im}[A_{\perp L}A_{tL}^* + (L\to R)]\right],$$

$$I_8 = \frac{\lambda_L}{\sqrt{2}q^4}[\mathrm{Im}(A_{0L}A_{\perp L}^*)+(L\to R)],$$

$$I_9 = \frac{\lambda_L}{q^4}\left[\mathrm{Im}(A_{\parallel L}^*A_{\perp L})+(L\to R)\right]. \tag{B.3}$$

The above expressions are modified if other BSM operators are included in the low-energy Hamiltonian, besides the ones in (3.1).

C Parametrization of the CKM and PMNS matrices

We use the standard parametrization of the CKM matrix

$$V_{\mathrm{CKM}} = \begin{pmatrix} c_{12}c_{13} & s_{12}c_{13} & s_{13}e^{-i\delta} \\ -s_{12}c_{23} - c_{12}s_{23}s_{13}e^{i\delta} & c_{12}c_{23} - s_{12}s_{23}s_{13}e^{i\delta} & s_{23}c_{13} \\ s_{12}s_{23} - c_{12}c_{23}s_{13}e^{i\delta} & -s_{23}c_{12} - s_{12}c_{23}s_{13}e^{i\delta} & c_{23}c_{13} \end{pmatrix}. \tag{C.1}$$

As four independent parameters we choose V_{us}, $|V_{cb}|$, $|V_{ub}|$ and the phase γ, so that

$$s_{13} = |V_{ub}|\,, \quad s_{12} = \frac{V_{us}}{c_{13}}\,, \quad s_{23} = \frac{|V_{cb}|}{c_{13}}\,, \quad \delta = \gamma\,,$$
$$c_{ij} = \sqrt{1-s_{ij}^2}\,. \tag{C.2}$$

V_{us} and γ are set to $V_{us} = 0.2253$ and $\gamma = 64.6°$. $|V_{cb}|$ and $|V_{ub}|$ are varied in the ranges spanned by the exclusive-inclusive measurements (4.1), with $|V_{cb}|_{\mathrm{exc}} = (39.1 \pm 0.5) \times 10^{-3}$, $|V_{cb}|_{\mathrm{inc}} = (42.19 \pm 0.78) \times 10^{-3}$, $|V_{ub}|_{\mathrm{exc}} = (3.51 \pm 0.12) \times 10^{-3}$, $|V_{ub}|_{\mathrm{inc}} = (4.19 \pm 0.17) \times 10^{-3}$ [5].

The standard parametrization is also used for the PMNS matrix

$$U_{\mathrm{PMNS}} = \begin{pmatrix} k_{12}k_{13} & x_{12}k_{13} & x_{13}e^{-i\delta_{\mathrm{PMNS}}} \\ -x_{12}k_{23} - k_{12}x_{23}x_{13}e^{i\delta_{\mathrm{PMNS}}} & k_{12}k_{23} - x_{12}x_{23}x_{13}e^{i\delta_{\mathrm{PMNS}}} & x_{23}k_{13} \\ x_{12}x_{23} - k_{12}k_{23}x_{13}e^{i\delta_{\mathrm{PMNS}}} & -x_{23}k_{12} - x_{12}k_{23}x_{13}e^{i\delta_{\mathrm{PMNS}}} & k_{23}k_{13} \end{pmatrix}, \tag{C.3}$$

where $x_{ij} = \sin\theta_{ij}$ and $k_{ij} = \cos\theta_{ij}$. A global fit of the parameters in (C.3) gives values which depend on the assumed hierarchy among the neutrino masses [102]: for normal ordering

$$\sin^2\theta_{12} = 0.308^{+0.012}_{-0.011}\,, \quad \sin^2\theta_{23} = 0.470^{+0.017}_{-0.013}\,, \quad \sin^2\theta_{13} = 0.02215^{+0.00056}_{-0.00058}\,,$$
$$\delta_{\mathrm{PMNS}} = (212^{+26}_{-41})°\,, \tag{C.4}$$

for inverted ordering

$$\sin^2\theta_{12} = 0.308^{+0.012}_{-0.011}\,, \quad \sin^2\theta_{23} = 0.550^{+0.012}_{-0.015}\,, \quad \sin^2\theta_{13} = 0.02231^{+0.00056}_{-0.00056}\,,$$
$$\delta_{\mathrm{PMNS}} = (274^{+22}_{-25})°\,. \tag{C.5}$$

The global fit in [103] gives consistent results. In the numerical analysis we use the parameters for normal ordering (C.4).

JHEP12(2025)069

Data Availability Statement. This article has no associated data or the data will not be deposited.

Code Availability Statement. This article has no associated code or the code will not be deposited.

References

[1] J. Aebischer, A.J. Buras, M. Cerdà-Sevilla and F. De Fazio, *Quark-lepton connections in Z' mediated FCNC processes: gauge anomaly cancellations at work*, JHEP **02** (2020) 183 [arXiv:1912.09308] [INSPIRE].

[2] A. Buras, *Gauge Theory of Weak Decays*, Cambridge University Press (2020) [DOI:10.1017/9781139524100] [INSPIRE].

[3] P. Colangelo, F. De Fazio, F. Loparco and N. Losacco, *Flavour anomalies, correlations, hadronic uncertainties, and all that*, Nuovo Cim. C **47** (2024) 145 [arXiv:2401.02796] [INSPIRE].

[4] B. Capdevila, A. Crivellin and J. Matias, *Review of semileptonic B anomalies*, Eur. Phys. J. ST **1** (2023) 20 [arXiv:2309.01311] [INSPIRE].

[5] Heavy Flavor Averaging Group (HFLAV) collaboration, *Averages of b-hadron, c-hadron, and τ-lepton properties as of 2023*, arXiv:2411.18639 [INSPIRE].

[6] P. Colangelo and F. De Fazio, *Tension in the inclusive versus exclusive determinations of $|V_{cb}|$: a possible role of new physics*, Phys. Rev. D **95** (2017) 011701 [arXiv:1611.07387] [INSPIRE].

[7] T. Kitahara, *Theoretical point of view on Cabibbo angle anomaly*, Int. J. Mod. Phys. A **39** (2024) 2442011 [arXiv:2407.00122] [INSPIRE].

[8] W. Altmannshofer et al., *Symmetries and Asymmetries of $B \to K^* \mu^+ \mu^-$ Decays in the Standard Model and Beyond*, JHEP **01** (2009) 019 [arXiv:0811.1214] [INSPIRE].

[9] Muon g-2 collaboration, *Final Report of the Muon E821 Anomalous Magnetic Moment Measurement at BNL*, Phys. Rev. D **73** (2006) 072003 [hep-ex/0602035] [INSPIRE].

[10] Muon g-2 collaboration, *Measurement of the Positive Muon Anomalous Magnetic Moment to 0.46 ppm*, Phys. Rev. Lett. **126** (2021) 141801 [arXiv:2104.03281] [INSPIRE].

[11] Muon g-2 collaboration, *Measurement of the Positive Muon Anomalous Magnetic Moment to 0.20 ppm*, Phys. Rev. Lett. **131** (2023) 161802 [arXiv:2308.06230] [INSPIRE].

[12] S. Borsanyi et al., *Leading hadronic contribution to the muon magnetic moment from lattice QCD*, Nature **593** (2021) 51 [arXiv:2002.12347] [INSPIRE].

[13] T. Aoyama et al., *The anomalous magnetic moment of the muon in the Standard Model*, Phys. Rept. **887** (2020) 1 [arXiv:2006.04822] [INSPIRE].

[14] CMD-3 collaboration, *Measurement of the $e^+e^- \to \pi+\pi-$ cross section from threshold to 1.2 GeV with the CMD-3 detector*, Phys. Rev. D **109** (2024) 112002 [arXiv:2302.08834] [INSPIRE].

[15] R. Aliberti et al., *The anomalous magnetic moment of the muon in the Standard Model: an update*, Phys. Rept. **1143** (2025) 1 [arXiv:2505.21476] [INSPIRE].

JHEP12(2025)069

[16] MUON G-2 collaboration, *Measurement of the Positive Muon Anomalous Magnetic Moment to 127 ppb*, Phys. Rev. Lett. **135** (2025) 101802 [arXiv:2506.03069] [INSPIRE].

[17] A.J. Buras and E. Venturini, *Searching for New Physics in Rare K and B Decays without $|V_{cb}|$ and $|V_{ub}|$ Uncertainties*, Acta Phys. Polon. B **53** (2021) 6 [arXiv:2109.11032] [INSPIRE].

[18] A.J. Buras and E. Venturini, *The exclusive vision of rare K and B decays and of the quark mixing in the standard model*, Eur. Phys. J. C **82** (2022) 615 [arXiv:2203.11960] [INSPIRE].

[19] A. Crivellin, G. D'Ambrosio and J. Heeck, *Explaining $h \to \mu^{\pm}\tau^{\mp}$, $B \to K^* \mu^+\mu^-$ and $B \to K\mu^+\mu^-/B \to Ke^+e^-$ in a two-Higgs-doublet model with gauged $L_\mu - L_\tau$*, Phys. Rev. Lett. **114** (2015) 151801 [arXiv:1501.00993] [INSPIRE].

[20] A. Crivellin, G. D'Ambrosio and J. Heeck, *Addressing the LHC flavor anomalies with horizontal gauge symmetries*, Phys. Rev. D **91** (2015) 075006 [arXiv:1503.03477] [INSPIRE].

[21] A. Crivellin et al., *Lepton-flavour violating B decays in generic Z' models*, Phys. Rev. D **92** (2015) 054013 [arXiv:1504.07928] [INSPIRE].

[22] C. Cornella et al., *Reading the footprints of the B-meson flavor anomalies*, JHEP **08** (2021) 050 [arXiv:2103.16558] [INSPIRE].

[23] M. Bordone, M. Rahimi and K.K. Vos, *Lepton flavour violation in rare Λ_b decays*, Eur. Phys. J. C **81** (2021) 756 [arXiv:2106.05192] [INSPIRE].

[24] D. Panda, M.K. Mohapatra and R. Mohanta, *Exploring the lepton flavor violating decay modes $b \to s\mu\pm\tau\mp$ in SMEFT approach*, Nucl. Phys. B **1008** (2024) 116720 [arXiv:2403.09393] [INSPIRE].

[25] D. Bečirević, F. Jaffredo, J.P. Pinheiro and O. Sumensari, *Lepton flavor violation in exclusive $b \to d\ell i\ell j$ and $b \to s\ell i\ell j$ decay modes*, Phys. Rev. D **110** (2024) 075004 [arXiv:2407.19060] [INSPIRE].

[26] A. Leike, *The phenomenology of extra neutral gauge bosons*, Phys. Rept. **317** (1999) 143 [hep-ph/9805494] [INSPIRE].

[27] P. Langacker and M. Plumacher, *Flavor changing effects in theories with a heavy Z' boson with family nonuniversal couplings*, Phys. Rev. D **62** (2000) 013006 [hep-ph/0001204] [INSPIRE].

[28] T. Appelquist, B.A. Dobrescu and A.R. Hopper, *Nonexotic Neutral Gauge Bosons*, Phys. Rev. D **68** (2003) 035012 [hep-ph/0212073] [INSPIRE].

[29] T.G. Rizzo, *Z' phenomenology and the LHC*, in the proceedings of the *Theoretical Advanced Study Institute in Elementary Particle Physics: Exploring New Frontiers Using Colliders and Neutrinos*, Boulder, U.S.A., June 04–30 (2006) [hep-ph/0610104] [INSPIRE].

[30] PARTICLE DATA GROUP collaboration, *Review of particle physics*, Phys. Rev. D **110** (2024) 030001 [INSPIRE].

[31] B. Holdom, *Two $U(1)$'s and Epsilon Charge Shifts*, Phys. Lett. B **166** (1986) 196 [INSPIRE].

[32] K.S. Babu, C.F. Kolda and J. March-Russell, *Leptophobic $U(1)$ s and the $R(b)$-$R(c)$ crisis*, Phys. Rev. D **54** (1996) 4635 [hep-ph/9603212] [INSPIRE].

[33] F. Del Aguila, M. Masip and M. Perez-Victoria, *Search for new neutral bosons at future colliders*, *Acta Phys. Polon. B* **27** (1996) 1469 [hep-ph/9603347] [INSPIRE].

[34] M. Carena, A. Daleo, B.A. Dobrescu and T.M.P. Tait, *Z' gauge bosons at the Tevatron*, Phys. Rev. D **70** (2004) 093009 [hep-ph/0408098] [INSPIRE].

[35] B.C. Allanach, J. Davighi and S. Melville, *An Anomaly-free Atlas: charting the space of flavour-dependent gauged $U(1)$ extensions of the Standard Model*, *JHEP* **02** (2019) 082 [*Erratum ibid.* **08** (2019) 064] [arXiv:1812.04602] [INSPIRE].

[36] A.J. Buras, M. Misiak, M. Munz and S. Pokorski, *Theoretical uncertainties and phenomenological aspects of $B \to X_s\gamma$ decay*, *Nucl. Phys. B* **424** (1994) 374 [hep-ph/9311345] [INSPIRE].

[37] M. Beneke, T. Feldmann and D. Seidel, *Systematic approach to exclusive $B \to Vl^+l^-$, $V\gamma$ decays*, *Nucl. Phys. B* **612** (2001) 25 [hep-ph/0106067] [INSPIRE].

[38] M. Misiak, *Radiative Decays of the B Meson: a Progress Report*, *Acta Phys. Polon. B* **49** (2018) 1291 [INSPIRE].

[39] P. Colangelo, G. Nardulli, N. Paver and Riazuddin, *Long Distance Effects in $b \to s$ Exclusive Decays*, *Z. Phys. C* **45** (1990) 575 [INSPIRE].

[40] C.S. Lim, T. Morozumi and A.I. Sanda, *A Prediction for $d\Gamma(b \to s\ell\bar{\ell})/dq^2$ Including the Long Distance Effects*, *Phys. Lett. B* **218** (1989) 343 [INSPIRE].

[41] N.G. Deshpande, J. Trampetic and K. Panose, *Resonance Background to the Decays $b \to s\ell^+\ell^-, B \to K^*\ell^+\ell^-$ and $B \to K\ell^+\ell^-$*, *Phys. Rev. D* **39** (1989) 1461 [INSPIRE].

[42] P.J. O'Donnell and H.K.K. Tung, *Resonance contributions to the decay $b \to s\ell^+\ell^-$*, *Phys. Rev. D* **43** (1991) 2067 [INSPIRE].

[43] N. Paver and Riazuddin, *On the interference between short distance and long distance contributions to $b \to s\ell^+\ell^-$*, *Phys. Rev. D* **45** (1992) 978 [INSPIRE].

[44] P. Colangelo, F. De Fazio, P. Santorelli and E. Scrimieri, *QCD sum rule analysis of the decays $B \to K\ell^+\ell^-$ and $B \to K^*\ell^+\ell^-$*, *Phys. Rev. D* **53** (1996) 3672 [*Erratum ibid.* **57** (1998) 3186] [hep-ph/9510403] [INSPIRE].

[45] M. Bordone, G. Isidori, S. Mächler and A. Tinari, *Short- vs. long-distance physics in $B \to K^{(*)}\ell^+\ell^-$: a data-driven analysis*, *Eur. Phys. J. C* **84** (2024) 547 [arXiv:2401.18007] [INSPIRE].

[46] A. Khodjamirian, T. Mannel, A.A. Pivovarov and Y.-M. Wang, *Charm-loop effect in $B \to K^{(*)}\ell^+\ell^-$ and $B \to K^*\gamma$*, *JHEP* **09** (2010) 089 [arXiv:1006.4945] [INSPIRE].

[47] A. Khodjamirian, T. Mannel and Y.M. Wang, *$B \to K\ell^+\ell^-$ decay at large hadronic recoil*, *JHEP* **02** (2013) 010 [arXiv:1211.0234] [INSPIRE].

[48] C. Bobeth, M. Chrzaszcz, D. van Dyk and J. Virto, *Long-distance effects in $B \to K^*\ell\ell$ from analyticity*, *Eur. Phys. J. C* **78** (2018) 451 [arXiv:1707.07305] [INSPIRE].

[49] M. Ciuchini et al., *Constraints on lepton universality violation from rare B decays*, *Phys. Rev. D* **107** (2023) 055036 [arXiv:2212.10516] [INSPIRE].

[50] LHCb collaboration, *Comprehensive analysis of local and nonlocal amplitudes in the $B^0 \to K^{*0}\mu^+\mu^-$ decay*, *JHEP* **09** (2024) 026 [arXiv:2405.17347] [INSPIRE].

[51] K. De Bruyn et al., *Branching Ratio Measurements of B_s Decays*, *Phys. Rev. D* **86** (2012) 014027 [arXiv:1204.1735] [INSPIRE].

[52] LHCb collaboration, *Precision measurement of CP violation in $B_s^0 \to J/\psi K^+K^-$ decays*, *Phys. Rev. Lett.* **114** (2015) 041801 [arXiv:1411.3104] [INSPIRE].

[53] J. Matias, F. Mescia, M. Ramon and J. Virto, *Complete Anatomy of $\bar{B}_d \to \bar{K}^{*0}(\to K\pi)l^+l^-$ and its angular distribution*, *JHEP* **04** (2012) 104 [arXiv:1202.4266] [INSPIRE].

JHEP12(2025)069

[54] A. Ali, T. Mannel and T. Morozumi, *Forward backward asymmetry of dilepton angular distribution in the decay $b \to s\ell^+\ell^-$*, Phys. Lett. B **273** (1991) 505 [INSPIRE].

[55] A. Ali, G.F. Giudice and T. Mannel, *Towards a model independent analysis of rare B decays*, Z. Phys. C **67** (1995) 417 [hep-ph/9408213] [INSPIRE].

[56] D.-S. Liu, *Estimates for forward-backward asymmetry in $B \to K^*(892)\ell^+\ell^-$*, Phys. Lett. B **346** (1995) 355 [hep-ph/9501276] [INSPIRE].

[57] A. Ali, P. Ball, L.T. Handoko and G. Hiller, *A comparative study of the decays $B \to (K, K^*)\ell^+\ell^-$ in standard model and supersymmetric theories*, Phys. Rev. D **61** (2000) 074024 [hep-ph/9910221] [INSPIRE].

[58] J. Charles et al., *Heavy to light form-factors in the heavy mass to large energy limit of QCD*, Phys. Rev. D **60** (1999) 014001 [hep-ph/9812358] [INSPIRE].

[59] M. Beneke and T. Feldmann, *Symmetry breaking corrections to heavy to light B meson form-factors at large recoil*, Nucl. Phys. B **592** (2001) 3 [hep-ph/0008255] [INSPIRE].

[60] F. Kruger and J. Matias, *Probing new physics via the transverse amplitudes of $B^0 \to K^{*0}(\to K^-\pi^+)l^+l^-$ at large recoil*, Phys. Rev. D **71** (2005) 094009 [hep-ph/0502060] [INSPIRE].

[61] D. Bečirević and E. Schneider, *On transverse asymmetries in $B \to K^*\ell^+\ell^-$*, Nucl. Phys. B **854** (2012) 321 [arXiv:1106.3283] [INSPIRE].

[62] M. Lindner, M. Platscher and F.S. Queiroz, *A Call for New Physics : The Muon Anomalous Magnetic Moment and Lepton Flavor Violation*, Phys. Rept. **731** (2018) 1 [arXiv:1610.06587] [INSPIRE].

[63] J. Hisano, T. Moroi, K. Tobe and M. Yamaguchi, *Lepton flavor violation via right-handed neutrino Yukawa couplings in supersymmetric standard model*, Phys. Rev. D **53** (1996) 2442 [hep-ph/9510309] [INSPIRE].

[64] R. Kitano, M. Koike and Y. Okada, *Detailed calculation of lepton flavor violating muon electron conversion rate for various nuclei*, Phys. Rev. D **66** (2002) 096002 [*Erratum ibid.* **76** (2007) 059902] [hep-ph/0203110] [INSPIRE].

[65] SINDRUM II collaboration, *Improved limit on the branching ratio of $\mu^- \to e^+$ conversion on titanium*, Phys. Lett. B **422** (1998) 334 [INSPIRE].

[66] J. Bernabeu, E. Nardi and D. Tommasini, *μ-e conversion in nuclei and Z' physics*, Nucl. Phys. B **409** (1993) 69 [hep-ph/9306251] [INSPIRE].

[67] T. Suzuki, D.F. Measday and J.P. Roalsvig, *Total Nuclear Capture Rates for Negative Muons*, Phys. Rev. C **35** (1987) 2212 [INSPIRE].

[68] SINDRUM II collaboration, *A search for muon to electron conversion in muonic gold*, Eur. Phys. J. C **47** (2006) 337 [INSPIRE].

[69] A.J. Buras, F. De Fazio and J. Girrbach, *The Anatomy of Z' and Z with Flavour Changing Neutral Currents in the Flavour Precision Era*, JHEP **02** (2013) 116 [arXiv:1211.1896] [INSPIRE].

[70] M. Blanke and A.J. Buras, *Emerging ΔM_d -anomaly from tree-level determinations of $|V_{cb}|$ and the angle γ*, Eur. Phys. J. C **79** (2019) 159 [arXiv:1812.06963] [INSPIRE].

[71] EOS Authors collaboration, *EOS: a software for flavor physics phenomenology*, Eur. Phys. J. C **82** (2022) 569 [arXiv:2111.15428] [INSPIRE].

[72] W. Altmannshofer and D.M. Straub, *New physics in $b \to s$ transitions after LHC run 1*, *Eur. Phys. J. C* **75** (2015) 382 [arXiv:1411.3161] [INSPIRE].

[73] B. Capdevila et al., *Patterns of New Physics in $b \to s\ell^+\ell^-$ transitions in the light of recent data*, *JHEP* **01** (2018) 093 [arXiv:1704.05340] [INSPIRE].

[74] M. Algueró et al., *$b \to s\ell^+\ell^-$ global fits after R_{K_S} and $R_{K^{*+}}$*, *Eur. Phys. J. C* **82** (2022) 326 [arXiv:2104.08921] [INSPIRE].

[75] M. Algueró et al., *To (b)e or not to (b)e: no electrons at LHCb*, *Eur. Phys. J. C* **83** (2023) 648 [arXiv:2304.07330] [INSPIRE].

[76] A. Bharucha, D.M. Straub and R. Zwicky, *$B \to V\ell^+\ell^-$ in the Standard Model from light-cone sum rules*, *JHEP* **08** (2016) 098 [arXiv:1503.05534] [INSPIRE].

[77] BaBar collaboration, *Measurements of branching fractions, rate asymmetries, and angular distributions in the rare decays $B \to K\ell^+\ell^-$ and $B \to K^*\ell^+\ell^-$*, *Phys. Rev. D* **73** (2006) 092001 [hep-ex/0604007] [INSPIRE].

[78] BaBar collaboration, *Measurement of angular asymmetries in the decays $B \to K^*\ell^+\ell^-$*, *Phys. Rev. D* **93** (2016) 052015 [arXiv:1508.07960] [INSPIRE].

[79] Belle collaboration, *Measurement of the Differential Branching Fraction and Forward-Backward Asymmetry for $B \to K^{(*)}\ell^+\ell^-$*, *Phys. Rev. Lett.* **103** (2009) 171801 [arXiv:0904.0770] [INSPIRE].

[80] Belle collaboration, *Lepton-Flavor-Dependent Angular Analysis of $B \to K^*\ell^+\ell^-$*, *Phys. Rev. Lett.* **118** (2017) 111801 [arXiv:1612.05014] [INSPIRE].

[81] CDF collaboration, *Measurements of the Angular Distributions in the Decays $B \to K^{(*)}\mu^+\mu^-$ at CDF*, *Phys. Rev. Lett.* **108** (2012) 081807 [arXiv:1108.0695] [INSPIRE].

[82] CMS collaboration, *Angular analysis of the decay $B^0 \to K^{*0}\mu^+\mu^-$ from pp collisions at $\sqrt{s} = 8$ TeV*, *Phys. Lett. B* **753** (2016) 424 [arXiv:1507.08126] [INSPIRE].

[83] CMS collaboration, *Measurement of angular parameters from the decay $B^0 \to K^{*0}\mu^+\mu^-$ in proton-proton collisions at $\sqrt{s} = 8$ TeV*, *Phys. Lett. B* **781** (2018) 517 [arXiv:1710.02846] [INSPIRE].

[84] ATLAS collaboration, *Angular analysis of $B_d^0 \to K^*\mu^+\mu^-$ decays in pp collisions at $\sqrt{s} = 8$ TeV with the ATLAS detector*, *JHEP* **10** (2018) 047 [arXiv:1805.04000] [INSPIRE].

[85] LHCb collaboration, *Differential branching fraction and angular analysis of the decay $B^0 \to K^{*0}\mu^+\mu^-$*, *JHEP* **08** (2013) 131 [arXiv:1304.6325] [INSPIRE].

[86] LHCb collaboration, *Measurement of Form-Factor-Independent Observables in the Decay $B^0 \to K^{*0}\mu^+\mu^-$*, *Phys. Rev. Lett.* **111** (2013) 191801 [arXiv:1308.1707] [INSPIRE].

[87] LHCb collaboration, *Angular analysis of the $B^0 \to K^{*0}\mu^+\mu^-$ decay using 3 fb^{-1} of integrated luminosity*, *JHEP* **02** (2016) 104 [arXiv:1512.04442] [INSPIRE].

[88] LHCb collaboration, *Measurement of CP-Averaged Observables in the $B^0 \to K^{*0}\mu^+\mu^-$ Decay*, *Phys. Rev. Lett.* **125** (2020) 011802 [arXiv:2003.04831] [INSPIRE].

[89] LHCb collaboration, *Angular Analysis of the $B^+ \to K^{*+}\mu^+\mu^-$ Decay*, *Phys. Rev. Lett.* **126** (2021) 161802 [arXiv:2012.13241] [INSPIRE].

[90] LHCb collaboration, *Amplitude Analysis of the $B^0 \to K^{*0}\mu^+\mu^-$ Decay*, *Phys. Rev. Lett.* **132** (2024) 131801 [arXiv:2312.09115] [INSPIRE].

JHEP12(2025)069

- [91] LHCb collaboration, *Search for the lepton-flavor violating decay $B_s^0 \to \phi\mu^\pm\tau^\mp$*, *Phys. Rev. D* **110** (2024) 072014 [arXiv:2405.13103] [INSPIRE].
- [92] LHCb collaboration, *Search for the lepton-flavour violating decays $B^0 \to K^{*0}\tau^\pm\mu^\mp$*, *JHEP* **06** (2023) 143 [arXiv:2209.09846] [INSPIRE].
- [93] Belle and Belle-II collaborations, *Search for lepton flavor-violating decay modes $B^0 \to K^{*0}\tau^\pm\ell^\mp(\ell = e, \mu)$ with hadronic B-tagging at Belle and Belle II*, *JHEP* **08** (2025) 184 [arXiv:2505.08418] [INSPIRE].
- [94] MEG II collaboration, *New limit on $\mu^+ \to e^+\gamma$ with the MEG II experiment*, *Eur. Phys. J. C* **85** (2025) 1177 [*Erratum ibid.* **85** (2025) 1317] [arXiv:2504.15711] [INSPIRE].
- [95] SINDRUM collaboration, *Search for the Decay $\mu^+ \to e^+e^+e^-$*, *Nucl. Phys. B* **299** (1988) 1 [INSPIRE].
- [96] P. Wintz, *Results of the SINDRUM-II experiment*, *Conf. Proc. C* **980420** (1998) 534 [INSPIRE].
- [97] MEG collaboration, *Search for the lepton flavour violating decay $\mu^+ \to e^+\gamma$ with the full dataset of the MEG experiment*, *Eur. Phys. J. C* **76** (2016) 434 [arXiv:1605.05081] [INSPIRE].
- [98] COMET collaboration, *COMET Phase-I Technical Design Report*, *PTEP* **2020** (2020) 033C01 [arXiv:1812.09018] [INSPIRE].
- [99] Mu2e collaboration, *Status and perspectives of cLFV at Mu2e*, *PoS* **WIFAI2023** (2024) 017 [INSPIRE].
- [100] R.M. Amarinei, *The Mu3e Experiment: Status and Short-Term Plans*, arXiv:2501.14667 [INSPIRE].
- [101] N. Gubernari, M. Reboud, D. van Dyk and J. Virto, *Dispersive analysis of $B \to K^{(*)}$ and $B_s \to \phi$ form factors*, *JHEP* **12** (2023) 153 [*Erratum ibid.* **01** (2025) 125] [arXiv:2305.06301] [INSPIRE].
- [102] I. Esteban et al., *NuFit-6.0: updated global analysis of three-flavor neutrino oscillations*, *JHEP* **12** (2024) 216 [arXiv:2410.05380] [INSPIRE].
- [103] F. Capozzi et al., *Neutrino masses and mixing: Entering the era of subpercent precision*, *Phys. Rev. D* **111** (2025) 093006 [arXiv:2503.07752] [INSPIRE].

JHEP12(2025)069